Photocatalysis on TiO$_2$ Surfaces: Principles, Mechanisms, and Selected Results

Amy L. Linsebigler, Guangquan Lu, and John T. Yates, Jr.*

Surface Science Center, Department of Chemistry, University of Pittsburgh, Pittsburgh, Pennsylvania 15260

Contents

1. Introduction

In 1972, Fujishima and Honda discovered the photocatalytic splitting of water on TiO$_2$ electrodes.[1] This event marked the beginning of a new era in heterogeneous photocatalysis. Since then, research efforts in understanding the fundamental processes and in enhancing the photocatalytic efficiency of TiO$_2$ have come from extensive research performed by chemists, physicists, and chemical engineers. Such studies are often related to energy renewal and energy storage.[2-6] In recent years, applications to environmental cleanup have been one of the most active areas in heterogeneous photocatalysis. This is inspired by the potential application of TiO$_2$-based photocatalysts for the total destruction of organic compounds in polluted air and wastewaters.[7-8]

In a heterogeneous photocatalysis system, photoinduced molecular transformations or reactions take place at the surface of a catalyst. Depending on where the initial excitation occurs, photocatalysis can be generally divided into two classes of processes. When the initial photoexcitation occurs in an adsorbate molecule which then interacts with the ground state catalyst substrate, the process is referred to as a catalyzed photoreaction. When the initial photo-
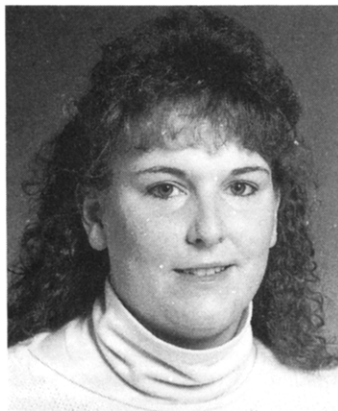
Amy Linsebigler received her B.S. degree in Chemistry from Seton Hill College in 1989. She is currently completing her Ph.D. in Chemistry at the University of Pittsburgh under the direction of Professor John T. Yates, Jr. During her doctoral studies she has examined several technologically important surface science systems. Her research includes the chemical reactivity of environmentally important adsorbates on metal surfaces, electronic modification of metal surfaces with thin metal films, and currently, the molecular level photochemistry and thermal chemistry of small probe molecules on metal oxide single-crystal surfaces.

Professor John T. Yates, Jr. began his research in surface chemistry as a graduate student at MIT. He continued this work from 1963 to 1982 at the National Bureau of Standards. In 1982 he founded the Surface Science Center at the University of Pittsburgh where he was appointed R.K. Mellon Professor. He now holds a joint appointment in the Departments of Chemistry and Physics. Work on metallic, semiconducting, and insulator surfaces is now underway using modern surface measurement techniques. His work with students and postdoctorals is focused on the use of electronic excitation to probe surface phenomena as well as the use of a range of surface vibrational spectroscopies and other methods for understanding surface processes.
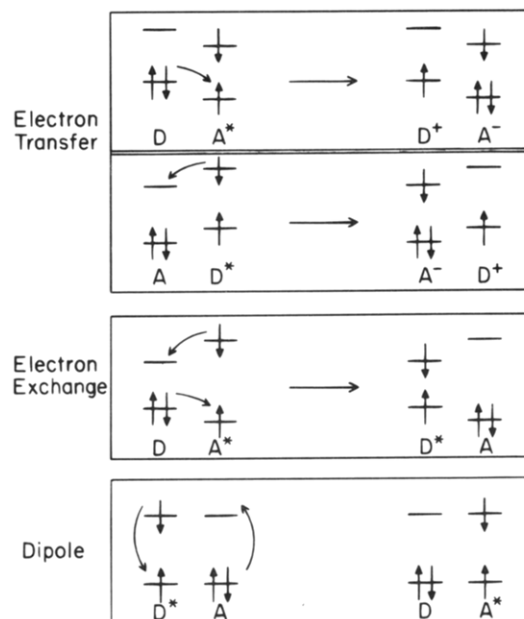
Guangquan Lu was born on July 24, 1965, in Shandong, the People's Republic of China. He received his B.S. in Chemistry from Shandong University in 1985, and his Ph.D. in Chemistry from the University of California at San Diego in 1992. His primary research interests are the kinetics and dynamics of thermal and photochemical processes on semiconductor surfaces. He has been involved in a broad range of research projects including the surface characterizations of Si/Ge chemical vapor depositions, the surface chemistry of photocatalytic reactions on TiO_2, and the surface and interface characterizations of advanced electronic materials processing. He is the recipient of the CGP scholarship from the Chinese Education Commission (1985), the American Vacuum Society Student Prize (1990), and the Russell and Sigurd Varian Fellow Award (1990).

Figure 1.1. Electron transfer and energy transfer processes.

excitation takes place in the catalyst substrate and the photoexcited catalyst then transfers an electron or energy into a ground state molecule, the process is referred to as a sensitized photoreaction.

The initial excitation of the system is followed by subsequent electron transfer and/or energy transfer. It is the subsequent deexcitation processes (via electron transfer or energy transfer) that leads to chemical reactions in the heterogeneous photocatalysis process. By using the electronic population changes in the molecular orbitals, Figure 1.1 schematically illustrates the different interactions between one reactive center in the excited state and another reactive center in the ground state. A reactive center can be a molecule or a surface reactive site.

An electron transfer process is a one-electron reaction in which an electron jumps from an occupied orbital of the donor reactant to the empty orbital of the acceptor reactant. The initial excitation may take place in either the donor molecule (D → D*) or the acceptor molecule (A → A*). The electron transfer process requires the overlap between the occupied donor orbital and the acceptor orbital which may be empty or half-filled. The electron transfer results in an ion pair of the donor cation (D$^+$) and the acceptor anion (A$^-$).

An energy transfer process takes place by electron exchange or dipole—dipole resonant coupling. These two processes operate through two fundamentally different mechanisms. Electron exchange occurs by two independent one-electron transfer steps—one in each direction. Both electron transfer and electron

exchange require orbital overlap between the interacting centers. When both processes are thermodynamically allowed, electron transfer predominates since the electron exchange process requires simultaneous overlap of two orbital pairs, whereas only one such overlap is necessary for electron transfer.[9] Dipole–dipole coupling occurs by a Coulombic resonance interaction in which the oscillating dipole of an excited state molecule is coupled with the induced dipole in a ground state quencher molecule. This coupling process does not require effective orbital overlap between the two interacting centers and can operate over a distance range from less than 10 Å to as large as 100 Å.[10]

There exists a vast body of literature dealing with the electron transfer and energy transfer processes in photocatalytic reactions. A detailed description of these processes is beyond the scope of this review. Several excellent review articles and books already exist.[11-19] Here, we tend to focus on interfacial processes and to summarize some of the operating principles of heterogeneous photocatalysis. In section 2, we will first look at the electronic excitation processes in a molecule and in a semiconductor substrate. The electronic interaction between the adsorbate molecule and the catalyst substrate will be discussed in terms of the catalyzed or sensitized photoreactions. In section 3, thermal and photocatalytic studies on TiO₂ are summarized with emphasis on the common characteristics and fundamental principles of the TiO₂-based photocatalysis systems. In section 4, we will address the research effort in the electronic modification of the semiconductor catalysts and its effect on the photocatalytic efficiency. Several representative examples will be presented including the Schottky barrier formation and modification at metal–semiconductor interfaces. Some concluding remarks and future research directions will be given in the final section.

2. Electronic Processes in Photocatalysis

2.1. Molecular Electronic Excitation

2.1.1. Molecular Spectroscopy and Photochemistry

Photocatalysis processes involve the initial absorption of photons by a molecule or the substrate to produce highly reactive electronically excited states. The efficiency of the photoinduced chemistry is controlled by the system's light absorption characteristics. In this section, we want to examine the factors that control the light absorption intensity by the molecule or by the substrate. We will first discuss the electronic excitation of a molecule upon photon absorption. The band-gap excitation of the semiconductor substrate will then be discussed and interfacial electron transfer will be reviewed.

Molecular electronic spectroscopy is a useful tool to determine where photochemistry may potentially occur.[11,12] Most importantly, we can determine what photon energy will most likely induce an electronic transition in a molecule based on whether the transition dipole moment μ_{if} will be zero for a transition from the initial state "i" to the final state "f". A transition that is forbidden by the selection rules is

expected to have no absorption intensity ($\mu_{if} = 0$), and it will therefore be unlikely to cause photochemical conversions which involve the excitation of such a transition.

The probability of an electronic transition can be calculated, using quantum mechanics purturbation theory, as being proportional to the square of the amplitude of the radiation field, E_0, and the square of the transition dipole moment, $|\mu_{if}|$:[20,21]

$$P \propto E_0{}^2 |\mu_{if}|^2 \tag{1}$$

Here $\mu_{if} = \langle \Psi_f | \mu | \Psi_i \rangle$ is the transition dipole moment for an electronic excitation process from the initial state Ψ_i to the final state Ψ_f. While the radiation field can be controlled by varying the light intensity, the transition dipole moment is an intrinsic property of the molecular structure.

According to the Born–Oppenheimer approximation, the molecular wave function Ψ can be expressed as the products of the electronic spatial wave function φ, the electronic spin wave function ς, and the nuclear wave function $\aleph$:[20,21]

$$\Psi = \varphi \cdot \varsigma \cdot \aleph \tag{2}$$

Then,

$$\mu_{if} = \langle \Psi_f | \mu | \Psi_i \rangle = \langle \varphi_f | \mu | \varphi_i \rangle \cdot \langle \varsigma_f | \varsigma_i \rangle \cdot \langle \aleph_f | \aleph_i \rangle \tag{3}$$

Now the transition dipole moment may be regarded as the product of the electronic transition moment, the electron spin wave function overlap, and the nuclear wave function overlap. The transition dipole moment, μ_{if}, will be zero if any of these three contributions become zero. This gives the selection rules for an electronic excitation process.

The electronic transition moment term $\langle \varphi_f | \mu | \varphi_i \rangle$ depends on the nature of the electron distributions in the initial and final electronic spatial wave functions. By examining the overall *symmetry* property of the spatial wave functions,[22,23] one can easily determine if this integral is zero. When this term is zero, the transition dipole moment μ_{if} is zero. Then the transition is a symmetry-forbidden transition.

The overlap integral of the spin wave functions $\langle \varsigma_f | \varsigma_i \rangle$ can be evaluated using the orthornormal property of the electron spin wave functions,[20] that is,

$$\langle \alpha | \alpha \rangle = \langle \beta | \beta \rangle = 1 \qquad \langle \alpha | \beta \rangle = \langle \beta | \alpha \rangle = 0 \tag{4}$$

Here α and β correspond to the only two spin configurations, spin-up (α) and spin-down (β). The electron spin functions maintain their orthogonality and normalization properties even when the electrons under consideration are described by different spatial wave functions. Using these properties, we can easily derive that the original spin orientation ς_i must be preserved in the final excited state in order to keep the term $\langle \varsigma_f | \varsigma_i \rangle$ nonzero. Therefore, singlet–singlet and triplet–triplet transitions are spin-allowed, while a singlet–triplet transition is spin-forbidden. Exceptions to this rule are often found among complex organic molecules containing heavy atoms (such as Br or I). Spin–orbit coupling induces weakly allowed singlet–triplet transitions in these systems.
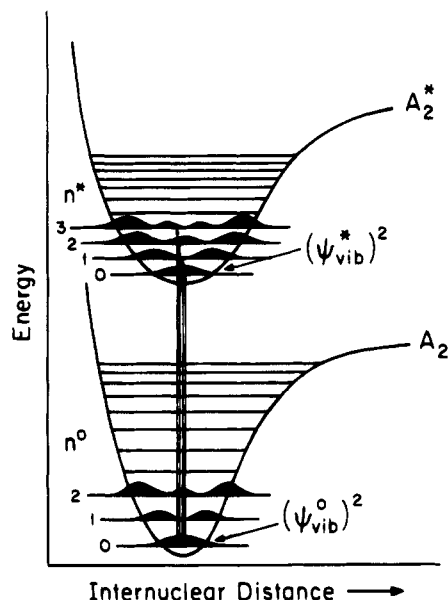
Figure 2.1. Vibronic transitions in a diatomic molecule.

The nuclear overlap integral $\langle \aleph_f | \aleph_i \rangle$ has to do with the nuclear motion (vibrational wave fuctions) during the electronic transition. Generally, the electronic transition induced by the absorption of a photon occurs much more rapidly than the nuclear motion. The nuclei remain essentially frozen at the equilibrium configuration of the ground state molecule during the transition. This is the Franck—Condon principle and is schematically illustrated in Figure 2.1.[21] Depending on the shape and spatial distribution of the nuclear wave functions of the initial and final states, the excited state can be produced with different vibrational and rotational levels. Then the nuclear overlap integral $\langle \aleph_f | \aleph_i \rangle$ can be used to determine which of the possible vibrational levels in the electronically excited state will be most likely populated during the transition. For a molecule with similar nuclear geometries in the ground and excited states, the largest overlap occurs when the vibrational quantum number (n^0) in the ground state and in the excited state remain the same $(\Delta n = 0)$. For a molecule that possesses a very different equilibrium nuclear geometry in the excited state, the largest overlap will occur at a different vibrational level.

Although the selection rules are often broken in the real world due to the simplicity of the molecular quantum mechanics formulations used to develop these selection rules, it is certainly true that a transition predicted to be forbidden will be very weak. These principles provide for us a set of generalities that we can use to understand patterns in experimental photochemistry. The excitation of a weak transition will not effectively induce a photochemical reaction in the sense that few of the delivered photons will actually be absorbed (low cross section). However, we must keep in mind that the reaction itself will be very efficient if each absorbed photon can lead to the the formation of a product molecule (high quantum yield). Thus, molecules with low absorption intensities are not necessarily poor photochemical reagents. The photochemical efficiency of an excitation will also be determined by which deexcitation channel is dominant, as discussed below.

2.1.2. Molecular Excitation and Deexcitation Events

The allowable excitation and deexcitation processes for a molecule are given in the energy level diagram in Figure 2.2. The ground state singlet energy level of the molecule is represented by S_0 and illustrates the energy of the molecule at room temperature in solution. The ground vibrational states for the three excited electronic states shown in Figure 2.2 for the molecule are represented as S_2 and S_1 for the singlet states and T_1 for the triplet state. The triplet excited state for the molecule is less energetic than the singlet excited state of the molecule. The respective energy levels of the excited states of the molecule are important when dealing with the photosensitization of semiconductors via dye molecule excitation. Numerous vibrational energy levels associated with the electronic energy levels exist but are not shown to simplify the figure. Absorption of radiation results in the excitation of the molecule from the ground state to one of the excited singlet states. The excitation to the second singlet state S_2 (requiring a shorter wavelength than excitation to S_1) is illustrated in Figure 2.2. The selection rules for an electronic excitation process imply that direct photoexcitation from the singlet ground state to the triplet excited state is spin forbidden [$\langle \varsigma_f | \varsigma_i \rangle = 0$]. The absorption
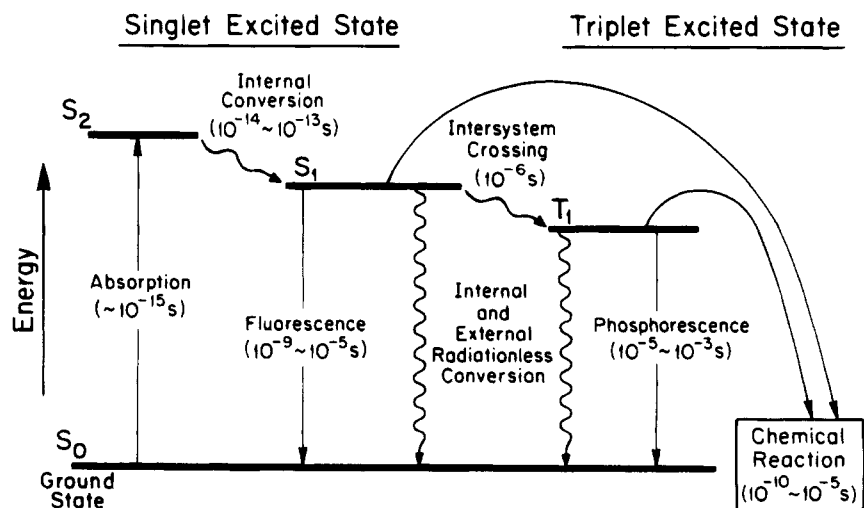
Figure 2.2. Excitation and deexcitation processes in a molecule.

of a photon of radiation occurs very rapidly, on the order of 10^{-15} s.[24a] Deexcitation events are much slower.

The deexcitation of the excited molecule favors the route which will minimize the lifetime of the excited state. Whether it occurs via emission of radiation such as fluorescence or phosphorescence, or a radiationless decay, indicated in Figure 2.2 as curvy lines, depends upon the competition between different decay channels. The lifetime of the excited state for fluorescence emission is 10^{-9} to 10^{-5} s.[24a]

After the excitation of a molecule from the ground state to a higher nondissociative excited state occurs, radiationless internal conversion transitions to the lower excited states usually take place before any radiative emission processes.[25] The conversion is observed when the upper electronic energy levels are close together and the vibrational energy levels overlap. The transition process from S_2 to S_1 is isoenergetic through overlay between vibrational levels. Once the transition occurs, the molecule undergoes vibrational relaxations to the ground vibrational state of the S_1 electronic excited state at a significant rate. Therefore, the S_2 to S_1 transition in Figure 2.2 represents a loss of energy for the internal conversion process. The time scale for internal conversion is 10^{-14} to 10^{-13} s.[24a] Internal as well as external conversions can also occur from the lowest excited states S_1 and T_1 to the ground state S_0. External conversions are the result of energy transfer to solvent or solute molecules and are usually only from the lowest excited states. If overlapping vibrational energy levels exist, deactivation via internal conversion to the ground state can occur faster than that involved in fluorescence emission.

Figure 2.2 represents excitation to bound upper electronic states for the purpose of illustrating the various classes of electronic transitions which are possible. Other upper states may involve chemical changes such as dissociation and are not shown here.

Intersystem crossing is a process in which the spin of the excited electron is reversed and the electrons become unpaired. Intersystem crossing is illustrated in Figure 2.2 between the S_1 and T_1 excited states. This process is the result of vibrational states overlapping. The time required for such a process is in the range of 10^{-6} s.[24a] Once intersystem crossing occurs from a singlet to a triplet excited state, the molecule undergoes deactivation by phosphorescence. The time scale for the radiative phosphorescence process is on the order of 10^{-5} to 10^{-3} s.[24a]

Relaxation of the excited singlet and triplet states can also occur by decomposition of the excited species to form new chemical species. Such reactions include photoinduced fragmentation, intramolecular transformation, and intermolecular and interfacial electron or energy transfer. The photochemical reactions occur on a time scale of 10^{-12} to 10^{-9} s.[24b]

2.2. Semiconductor Electronic Excitation

2.2.1. Band-Gap Photoexcitation

Unlike metals which have a continuum of electronic states, semiconductors possess a void energy region where no energy levels are available to promote recombination of an electron and hole produced by photoactivation in the solid. The void region which extends from the top of the filled valence band to the bottom of the vacant conduction band is called the band gap. Once excitation occurs across the band gap there is a sufficient lifetime, in the nanosecond regime,[26] for the created electron−hole pair to undergo charge transfer to adsorbed species on the semiconductor surface from solution or gas phase contact. If the semiconductor remains intact and the charge transfer to the adsorbed species is continuous and exothermic the process is termed heterogeneous photocatalysis.

The initial process for heterogeneous photocatalysis of organic and inorganic compounds by semiconductors is the generation of electron−hole pairs in the semiconductor particles. The enlarged section of Figure 2.3 shows the excitation of an electron from the valence band to the conduction band initiated by light absorption with energy equal to or greater than
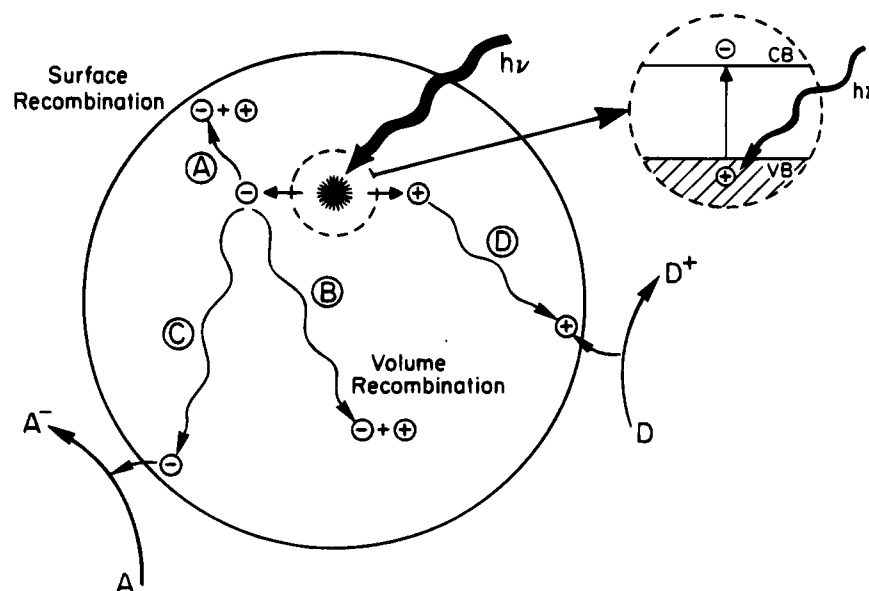
Figure 2.3. Schematic photoexcitation in a solid followed by deexcitation events.

the band gap of the semiconductor. Upon excitation, the fate of the separated electron and hole can follow several pathways. Figure 2.3 illustrates some of the deexcitation pathways for the electrons and holes.

The photoinduced electron transfer to adsorbed organic or inorganic species or to the solvent results from migration of electrons and holes to the semiconductor surface. The electron transfer process is more efficient if the species are preadsorbed on the surface.[27] While at the surface the semiconductor can donate electrons to reduce an electron acceptor (usually oxygen in an aerated solution) (pathway C); in turn, a hole can migrate to the surface where an electron from a donor species can combine with the surface hole oxidizing the donor species (pathway D). The probability and rate of the charge transfer processes for electrons and holes depends upon the respective positions of the band edges for the conduction and valence bands and the redox potential levels of the adsorbate species.

In competition with charge transfer to adsorbed species is electron and hole recombination. Recombination of the separated electron and hole can occur in the volume of the semiconductor particle (pathway B) or on the surface (pathway A) with the release of heat. The process of back-donation after charge transfer from the adsorbed species to the semiconductor surface can occur but is not illustrated in Figure 2.3.

The efficiency of the photocatalytic process is measured as a quantum yield which is defined as the number of events occurring per photon absorbed. The ability to measure the actual absorbed light is very difficult in heterogeneous systems due to scattering of light by the semiconductor surface. It is usually assumed that all the light is absorbed and the efficiency is quoted as an apparent quantum yield. If several products are formed from the photocatalytic reaction then the efficiency is sometimes measured as the yield of a particular product.

To determine the efficiency or quantum yield, a combination of all the pathway probabilities for the electron and hole must be considered. The quantum yield for an ideal system, ϕ, given by the simple relationship:

$$\phi \propto \frac{k_{CT}}{k_{CT} + k_R} \tag{5}$$

is proportional to the rate of the charge transfer processes (k_{CT}) and inversely proportional to the sum of the charge transfer rate (k_{CT}) and the electron–hole recombination rate (k_R) (bulk and surface). It is assumed that diffusion of the products into the solution occurs quickly without the reverse reaction of electrons recombining with donors and holes recombining with acceptors. Without recombination the quantum yield would take on the ideal value of 1 for the photocatalytic process. In this case the rate of charge transfer would be dependent on the diffusion of charge carriers to the surface in the absence of excess surface charge. However, this is an idealization. In a real system recombination does occur and the concentration of electrons (n_s) and holes (p_s) at the surface is not equal.[28] For example, charge
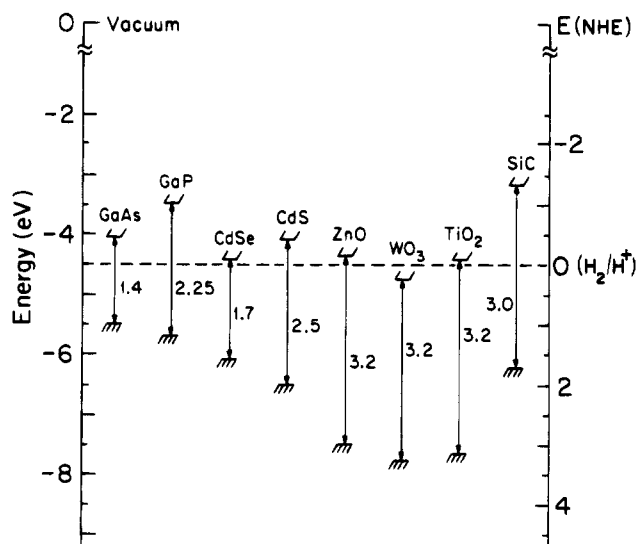
Figure 2.4. Energies for various semiconductors in aqueous electrolytes at pH = 1.

carrier traps are used to promote the trapping of electrons and holes at the surface leading to a more efficient charge transfer process. For photooxidation processes on TiO_2, $n_s > p_s$, because the electron transfer process to molecular oxygen trapped at defect sites is relatively slow.[28]

Obviously electron and hole recombination is detrimental to the efficiency of a semiconductor photocatalyst. Modifications to semiconductor surfaces such as addition of metals, dopants, or combinations with other semiconductors are beneficial in decreasing the electron and hole recombination rate and thereby increasing the quantum yield of the photocatalytic process. Such semiconductor modifications will be discussed in detail in section 4 later in the review.

2.2.2. Band-Edge Positions

The ability of a semiconductor to undergo photoinduced electron transfer to adsorbed species on its surface is governed by the band energy positions of the semiconductor and the redox potentials of the adsorbate. The relevant potential level of the acceptor species is thermodynamically required to be below (more positive than) the conduction band potential of the semiconductor. The potential level of the donor needs to be above (more negative than) the valence band position of the semiconductor in order to donate an electron to the vacant hole.

The band edge positions of several semiconductors are presented in Figure 2.4. The internal energy scale is given on the left for comparison to the vacuum level and on the right for comparison to normal hydrogen electrode (NHE). The positions are derived from the flat band potentials in a contact solution of aqueous electrolyte at pH = 1. The pH of the electrolyte solution influences the band edge positions of the various semiconductors compared to the redox potentials for the adsorbate.

2.2.3. Charge Carrier Trapping

Recombination of the photoexcited electron–hole pair needs to be retarded for an efficient charge
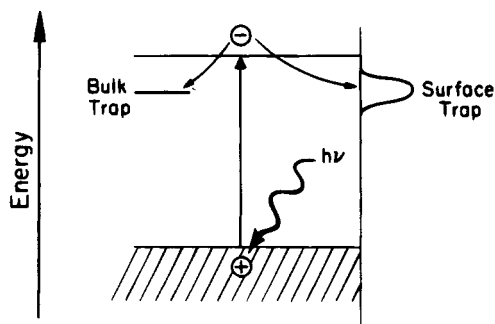
Figure 2.5. Surface and bulk electron carrier trapping.

transfer process to occur on the photocatalyst surface. Charge carrier trapping would suppress recombination and increase the lifetime of the separated electron and hole to above a fraction of a nanosecond. In the preparation of colloidal and polycrystalline photocatalysts, ideal crystal lattices of the semiconductors are not produced. Instead, surface and bulk irregularities naturally occur during the preparation process. The irregularities are associated with surface electron states which differ in their energy from the bands present in the bulk semiconductor. The electron states serve as charge carrier traps and help suppress the recombination of electrons and holes.

The nature of surface defect sites depends on the method of chemical preparation. As a specific example of the role of surface traps, CdS colloids produced by adding H$_2$S to a cadmium salt solution possess surface defect sites which promote radiationless recombination of charge carriers. The radiationless recombination process dominates in this semiconductor system. The fluorescence spectrum of this colloidal suspension exhibits only a very weak red fluorescence peak at a photon energy 0.4 eV below the absorption threshold. The decrease in energy is due to the trapping of charge carriers on the surface at energy levels below the conduction band edge. After modifying the surface by addition of excess Cd^{2+} ions and an adjustment in pH toward a basic solution, the maximum of fluorescence occurs at the absorption threshold (2.48 eV). The surface modification blocks defect trap sites which also promote radiationless recombination of charge carriers. The high quantum yield (50%) for fluorescence on the modified CdS is a result of electron–hole pair recombination across the bulk band gap.[29]

A simplified illustration of available bulk and surface trapping states for a photogenerated electron in a semiconductor is shown in Figure 2.5. In this illustration, the energy levels of the bulk and surface state traps fall within the band gap of the semiconductor. These surface and bulk states are localized. The charge carriers trapped in such states are localized to a particular site on the surface or in the bulk. The population of bulk and surface traps is dependent on the energy difference between the trap and the bottom of the conduction band and the decrease in entropy when the electron undergoes trapping. Experimentally, trapping of conduction band electrons generated by picosecond laser photolysis of colloidal TiO$_2$ has been observed. Time-resolved transient absorption of trapped electrons have demonstrated a lifetime in the nanosecond time

range.[30] The trapping of valence band holes required an average time of 250 ns. Electron paramagnetic resonance (EPR) spectroscopy experiments of illuminated colloidal TiO$_2$ at 4.2 K have shown the existence of trapped photogenerated electrons (to form Ti^{3+} defect sites) within the bulk of the semiconductor.[31] Adsorbed oxygen on the TiO$_2$ surface scavenges the trapped electrons and inhibits the formation of Ti^{3+} sites. Trapped holes are also observed. The exact species associated with the trapped hole is undetermined, although O$^-$, O$_3^-$, and ·OH species are postulated to exist in various cases.

Further illustrations of the nature and role of defect sites are given in sections 3.1 and 3.2.

2.2.4. Quantum Size Effects

Size quantization effects for metals and semiconductors have recently been a subject of great interest, and several reviews are available.[32-36] Quantum size effects (QSE) occur for semiconductor particles (Q-particles) on the order of 10–100 Å in size. The anomalies arise when the size of the semiconductor particles become comparable to the de Broglie wavelength of the charge carriers in the semiconductor. The range of size for particles experiencing QSE is therefore dependent on the effective mass for the Q-particle semiconductor. The electron and hole produced in Q-particles are confined in a potential well of small geometrical dimensions. The electron and hole do not experience the electronic delocalization present in a bulk semiconductor possessing a conduction band and a valence band. Instead, the confinement produces a quantization of discrete electronic states and increases the effective band gap of the semiconductor. Such effects can change the color of the material (due to the altered optical absorption maxima) and the photocatalytic properties.

Recent advances in the ability to synthesize cluster particles allows the study of size-dependent anomalies compared to the bulk properties.[29,33,37,38] CdS,[29,39,40] ZnO,[41] and PbS[42] are the Q-particles studied in the most detail both experimentally and theoretically. Figure 2.6 illustrates the increase in effective band gap for CdS when the size of the particles is decreased from $d > 100$ Å, signifying the dimensions of a bulk semiconductor, to $d \sim 26$ Å where significant quantum size effects occur for CdS.[39,40] This
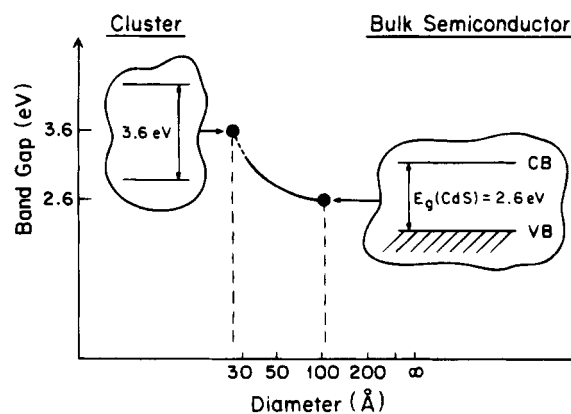
Figure 2.6. Quantum size effect on semiconductor band gap.

quantization and increase in effective band gap is observed experimentally as a blue shift in the absorption and emission spectra for CdS. The energy shift in the band gap, ΔE, as a function of particle size can be predicted by the three dimensional confinement model based on the effective mass approximation:[39,40,43-45]

$$\Delta E = \frac{\hbar^2 \pi^2}{2R^2}\left[\frac{1}{m_e^*} + \frac{1}{m_h^*}\right] - \frac{1.786e^2}{\epsilon R} - 0.248E_{RY} \quad (6)$$

where R is the particle radius, m_e^* and m_h^* are the effective masses for the electrons and holes, ϵ is the dielectric constant, and E_{RY} is the effective Rydberg energy given as $e^4/2\epsilon^2\hbar^2(1/m_e^* + 1/m_h^*)$. The equation is characterized by the first term which represents the energy of localization, the second term which represents the Coulombic attraction,[39,40] and the third term which represents the correlation effect.[46] ΔE gives the blue shift in the band gap of the particle:

$$E_{TE} = \Delta E + E_g^{bulk} \quad (7)$$

and determines the transition energy (effective band gap), E_{TE}, for the particle.

The increase in effective band gap and consequently the blue shift in the absorption threshold, can become quite dramatic for bulk semiconductors with very small band gaps. The band gap for PbS (E_g (bulk) = 0.4 eV) can actually be increased by a factor of 6 when the particle size is decreased from 150 to 13 Å. When the Q-particle sizes are less than 13 Å, discrete absorption bands are observed in the absorption spectrum for PbS. A theoretical treatment for PbS has shown that the simple confinement model using the effective mass approximations cannot reproduce the experimental results.[42] Other theoretical treatments have also been developed to fit the experimental data for the very small diameter particles <15 Å. While photocatalyst particles have not reached Q-particle sizes yet, it can be expected that this may happen in the future as new materials are produced.

2.2.5. Band Bending and Formation of Schottky Barrier

Contact between a semiconductor and another phase (i.e. liquid, gas, or metal) generally involves a redistribution of electric charges and the formation of a double layer. The transfer of mobile charge carriers between the semiconductor and the contact phase, or the trapping of charge carriers at surface states at the interface, produces a space charge layer. For semiconductor–gas phase interactions, an n-type semiconductor such as TiO$_2$ can have surface states available for electron trapping. The surface region will become negatively charged. To preserve electrical neutrality a positive space charge layer develops just within the semiconductor causing a shift in electrostatic potential and a bending of bands upward toward the surface.

Figure 2.7 illustrates the space charge layers produced from the mobility of charge across a semiconductor–solution interface for an n-type semiconductor.[15] Part a of Figure 2.7 shows the flat band potential diagram in the absence of a space charge
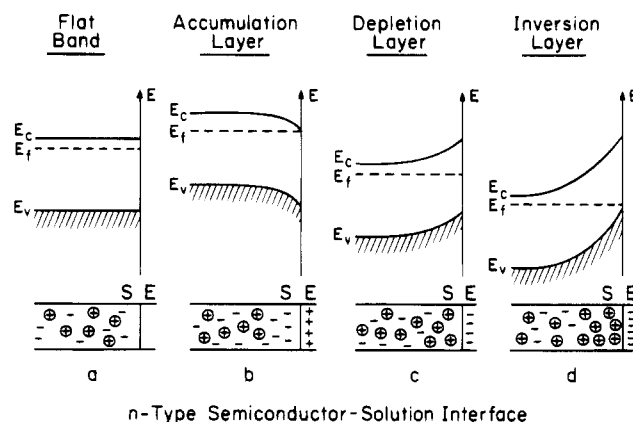
Figure 2.7. Space charge layer formation and band bending.
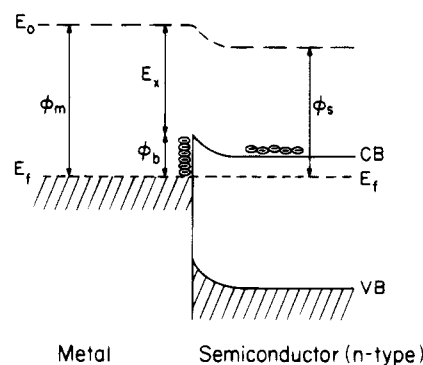
Figure 2.8. Schematic of Schottky barrier.

layer. The semiconductor contains a uniform distribution of charge. The existence of a positive charge on the interface (part b) increases the majority carrier concentration of electrons near the surface within the region of the space charge layer. The space charge layer formed is called an accumulation layer. The bands of the semiconductor will bend down as one moves toward the surface as a result of the decrease of electron potential energy as one moves toward the positively charged outerlayer. When negative charges accumulate at the interface the majority electron carrier concentration is less than in the interior of the semiconductor (part c). The space charge layer formed is a depletion layer and the bands bend upward toward the surface. When the depletion of the majority charge carriers extends far into the semiconductor, the Fermi level can decrease below the intrinsic level, which is half way between the bottom of the conduction band and the top of the valence band. The surface region of the semiconductor appears to be p-type while the bulk still exhibits n-type behavior. This space charge layer is called an inversion layer (part d).

The semiconductor–metal system represents a good example illustrating space charge layers, band bending, and the formation of a Schottky barrier as shown in Figure 2.8. Electrically neutral and isolated from each other, the metal and the n-type semiconductor have different Fermi level positions.[47] In the case to be discussed here, the metal has a higher work function (ϕ_m) than the semiconductor (ϕ_s). When the two materials are connected electrically, electron migration from the semiconductor to the metal occurs until the two Fermi levels are

aligned as shown in Figure 2.8. The electrical contact has formed a space charge layer. The surface of the metal acquires an excess negative charge while the semiconductor exhibits an excess positive charge as a result of electron migration away from the barrier region. The bands of the semiconductor bend upward toward the surface, and the layer is said to be depleted. The barrier formed at the metal—semiconductor interface is called the Schottky barrier. The height of the barrier, ϕ_b, is given by

$$\phi_b = \phi_m - E_x \qquad (8)$$

where E_x is the electron affinity, measured from the conduction band edge to the vacuum level of the semiconductor. The diagram in Figure 2.8 illustrates an ideal metal—semiconductor contact, i.e. no surface states exist on the semiconductor, etc. The Schottky barrier produced at the metal—semiconductor interface can serve as an efficient electron trap preventing electron—hole recombination in photocatalysis as discussed in section 4.2.

2.3. Photoinduced Electron Transfer Processes on the Surface of Catalysts

In an electronically excited state, a molecule or semiconductor particle becomes highly reactive. Electron transfer occurs between molecules at the surface or between a surface site and an adsorbate molecule. Similar to the classification of photocatalysis, electron transfer processes can also be broadly divided into two general categories as shown in Figure 2.9, parts I and II. The categories involve either excitation of the adsorbate directly by the photon or excitation of the solid by the photon followed by excitation of the adsorbate.

For a catalyst substrate with no accessible energy levels for the adsorbate, such as SiO_2 and Al_2O_3, only a 2D environment is provided for the reactant molecules, and the solid does not participate in the photoinduced electronic process.[48] Electron transfer occurs directly from the adsorbed donor molecule to the acceptor molecule as shown in Figure 2.9I, part A. When there are accessible energy levels in the substrate and there is strong electronic interaction between the substrate and the adsorbate, the electron transfer may be mediated by the substrate. An electron is transferred from the donor into a substrate level and then into the acceptor orbital, as shown in Figure 2.9I, part B. This scheme operates in the photosensitization of semiconductor particles by dye molecules, as will be discussed in section 4.4. An electron is injected from the excited state dye molecule into the semiconductor particle which then reduces another adsorbate molecule.[49]

In Figure 2.9II, part C, the initial excitation takes place in the substrate. For a semiconductor, an electron is excited into the conduction band of the semiconductor, leaving a positively charged hole at the band edge of the valence band. An electron is transferred into the empty acceptor orbital from the catalyst conduction band. Simultaneously, an electron is donated from the filled donor orbital to recombine with the hole at the valence band edge. This case is generally seen in most photocatalysis

processes on wide band-gap oxide semiconductor surfaces, and is the focus of the rest of this review. Figure 2.9I, part D shows a common excitation scheme observed for adsorbates on metals. When the metal is irradiated, a hot electron is generated at a level above the Fermi edge and this electron then tunnels into an empty level in the adsorbate molecule. Processes occurring by this type of electron transfer process have been reviewed recently.[50]

The interfacial electron transfer process has been extensively investigated[14,15] and the dynamics of such processes continue to attract intensive research effort.[51-54] The rate constant for an interfacial electron transfer is found to be greater than 5×10^{10} s^{-1}.[55,56] The driving force for the heterogeneous electron transfer is the energy difference between the conduction band of the semiconductor and the reduction potential of the acceptor redox couple, A/A⁻, ($\Delta E = E_{cb} - E_{A/A^-}$). An excellent review of this subject has been written by Lewis,[57] and applications of these ideas are given in section 3.6 dealing with photooxidation processes at the liquid—solid interface of TiO_2.
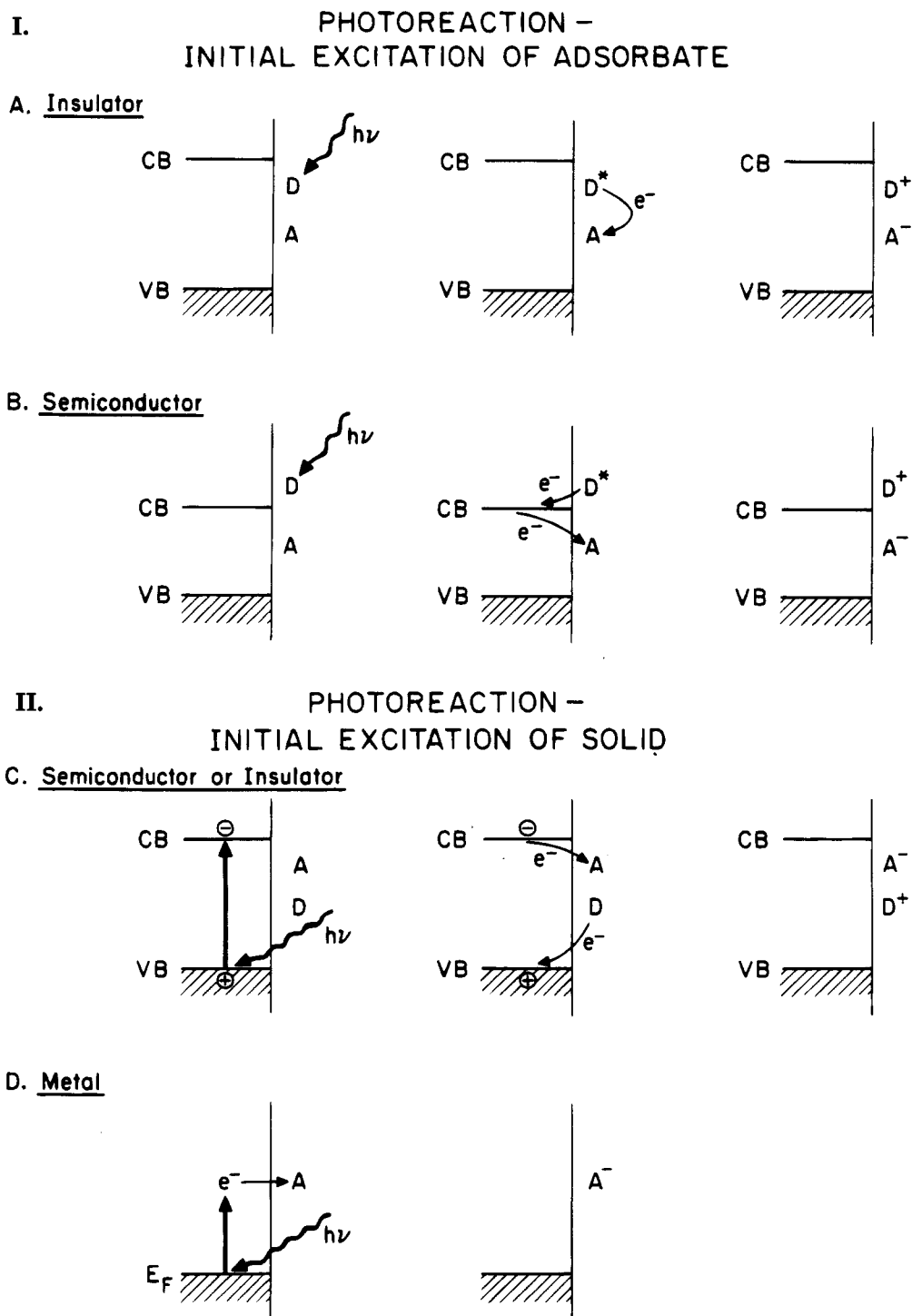
3. Photocatalysis on TiO₂

3.1. The Lattice and Electronic Structure of TiO₂

3.1.1. The Lattice Structure of Rutile and Anatase

Two different crystal structures of TiO_2, rutile and anatase, are commonly used in photocatalysis, with anatase showing a higher photocatalytic activity.[58] The structure of rutile and anatase can be described in terms of chains of TiO_6 octahedra. The two crystal structures differ by the distortion of each octahedron and by the assembly pattern of the octahedra chains. Figure 3.1 shows the unit cell structures of the rutile and anatase crystals.[59-61] Each Ti^{4+} ion is surrounded by an octahedron of six O^{2-} ions. The octahedron in rutile is not regular, showing a slight orthorhombic distortion. The octahedron in anatase is significantly distorted so that its symmetry is lower than orthorhombic. The Ti—Ti distances in anatase are greater (3.79 and 3.04 Å vs 3.57 and 2.96 Å in rutile) whereas the Ti—O distances are shorter than in rutile (1.934 and 1.980 Å in anatase vs 1.949 and 1.980 Å in rutile).[60] In the rutile structure each octahedron is in contact with 10 neighbor octahedrons (two sharing edge oxygen pairs and eight sharing corner oxygen atoms) while in the anatase structure each octahedron is in contact with eight neighbors (four sharing an edge and four sharing a corner). These differences in lattice structures cause different mass densities and electronic band structures between the two forms of TiO_2, as indicated in Figure 3.1.

3.1.2. Geometric and Electronic Structure of TiO₂ Single-Crystal Surfaces

The surface structure of rutile single crystals have been studied with the rutile (110) surface being most extensively investigated. Figure 3.2 shows the model structures for the $TiO_2(110)$ surface. This surface is thermodynamically most stable. Other faces will reconstruct upon heating to high temperatures to produce (110) facets.[62] The structure of three types of oxygen vacancy sites are also shown in the figure.

I.

PHOTOREACTION –
INITIAL EXCITATION OF ADSORBATE

A. Insulator

CB — D $h\nu$ CB — D* e⁻   CB — D⁺

A   A   A⁻

VB   VB   VB

B. Semiconductor

CB — D $h\nu$ CB — e⁻ D*   CB — D⁺

A   e⁻ A   A⁻

VB   VB   VB

II.

PHOTOREACTION –
INITIAL EXCITATION OF SOLID

C. Semiconductor or Insulator

CB — ⊖   A   CB — ⊖   e⁻ A   CB — A⁻

D   D   D⁺

VB ⊕ $h\nu$ VB ⊕   e⁻   VB

D. Metal

e⁻ → A

$h\nu$

E_F

A⁻

Figure 2.9. (I) Catalyzed photoreaction, initial excitation of adsorbate, and (II) Sensitized photoreaction, initial excitation of solid.

The electronic structure of the nearly perfect TiO_2 surfaces is essentially identical to that of the bulk rutile TiO_2. Figure 3.3 shows the photoemission spectra from vacuum-fractured (110), (100), and (001) faces of rutile TiO_2.[63] All three faces give spectra similar to that of the bulk. The intense peak at ~ 6 eV is due to electron emission from the O 2p obitals. The small emission peak near the Fermi level is due to point defect oxygen vacancies. This feature is more clearly shown in Figure 3.4. Figure 3.4 shows the electronic band structure constructed from photoemission (UPS) and inverse photoemission (IPS) spectra for a slightly defective $TiO_2(110)$ surface.[64]

The filled valence band at ~ 6 eV is composed of O 2p orbitals (as shown in the UPS spectrum) and the empty conduction band is composed of Ti 3d, 4s, and 4p orbitals. The Ti 3d orbitals dominate the lower portion of the conduction band. The weak emission at ~ 0.8 eV below the Fermi level is associated with the defect induced-Ti 3d-derived levels. This state can be eliminated by surface oxidation.

Few studies have been conducted on the structure of the anatase single crystal surfaces.[60,61,65] A recent photoemission study by Sanjines et al.[65] has shown that anatase $TiO_2(101)$ and polycrystalline anatase thin films exhibit similar electronic photoemission
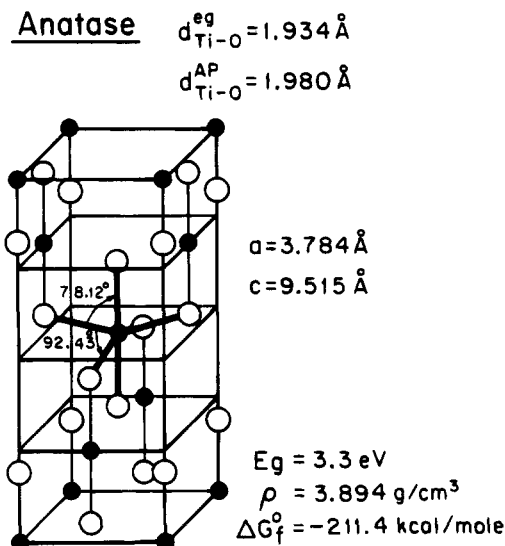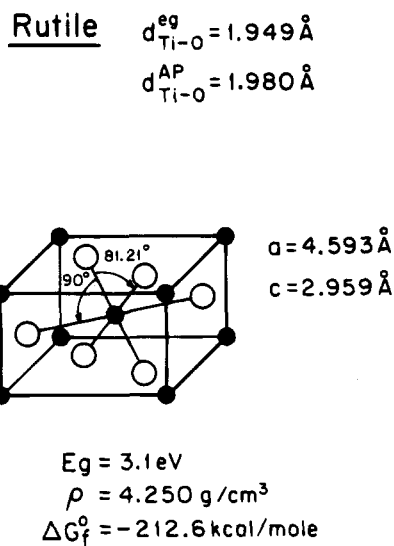
Rutile $d^{eg}_{Ti-O} = 1.949 Å$
$d^{AP}_{Ti-O} = 1.980 Å$

$a = 4.593 Å$
$c = 2.959 Å$

$Eg = 3.1 eV$
$\rho = 4.250 g/cm^3$
$\Delta G^o_f = -212.6 kcal/mole$

Anatase $d^{eg}_{Ti-O} = 1.934 Å$
$d^{AP}_{Ti-O} = 1.980 Å$

$a = 3.784 Å$
$c = 9.515 Å$

$Eg = 3.3 eV$
$\rho = 3.894 g/cm^3$
$\Delta G^o_f = -211.4 kcal/mole$

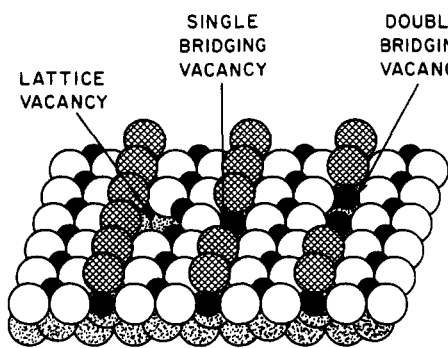**Figure 3.1.** Structure of rutile and anatase TiO₂.
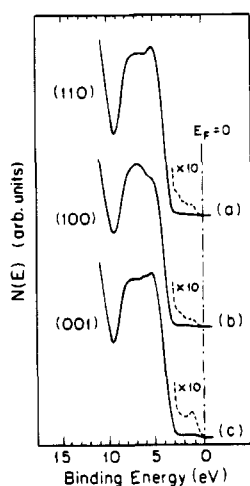
Figure 3.2. Defect sites of TiO₂(110).

Figure 3.3. Photoemission spectra for vacuum-fractured TiO₂(110), (100), (001) surfaces.

behavior to that of rutile. A similar 0.8 eV emission feature was observed upon the introduction of Ti³⁺ defect sites by sputtering or H₂ reduction.

3.2. Chemisorption Studies on TiO₂ Surfaces

The chemisorption properties on TiO₂ surfaces have been extensively studied. Particular interest has been given to the influence of defect sites on the chemisorptive behavior of the surface. Since these defect sites are also found as the active sites for photocatalytic processes,[66] we will in this section
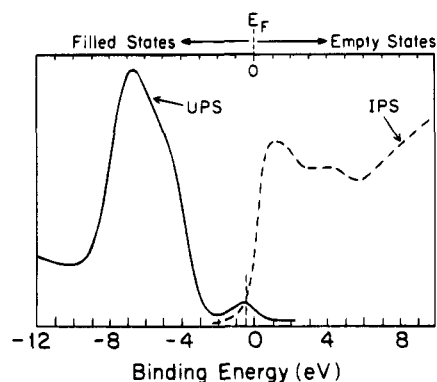
Figure 3.4. Photoemission and inverse photoemission spectra on a slightly defective TiO₂(110) surface.

briefly summarize the results of recent chemisorption studies and try to illustrate some of the common characteristics of the TiO₂ surfaces.

3.2.1. Water Adsorption

Much of the interest in studying the interaction of water with TiO₂ surfaces was stimulated by the discovery of the photocatalytic splitting of water on TiO₂ electrodes.[1] Efforts have been focused on what forms of water (molecular or dissociated) exist on the surface and what are the important parameters in controlling the adsorption behavior. Henrich et al. detected surface hydroxyl groups present after H₂O adsorption at 300 K on a slightly defective TiO₂(110) surface with photoemission (UPS).[67] This result was confirmed in a synchrotron photoemission study by the Madey group.[68,69] The amount of water dissociatively adsorbed at 300 K was well below one monolayer and the coverage of OH(a) was found to be independent of the coverage of surface oxygen vacancy defect sites. In fact, surface defect coverage was found to slightly increase during H₂O adsorption.[68] On the basis of these results, it was proposed that an adsorbed H₂O molecule reacts with a bridging-oxygen atom to form two OH groups. It was also found that molecular water adsorption occurs below 160 K and hydroxyl groups were produced by water dissociation upon heating the physisorbed layer to

above 200 K.[68] However, most of the adsorbed water desorbs molecularly between 170–180 K. The hydroxyls were not completely removed from the surface until 350–400 K.

A recent XPS and TPD study by Hugenschmidt et al.[70] reported four different adsorption states for H_2O on $TiO_2(110)$, a 500 K TPD peak due to surface hydroxyls bound to oxygen vacancies, a 375 K peak due to dissociated H_2O, a 250–300 K feature due to molecular H_2O adsorbed at Ti^{4+} sites, a 170 K desorption feature due to molecular H_2O bound to bridging-oxygen anion sites, and a 160 K mutilayer state. The assignments of the 250–300 K and the 170 K peaks are inconsistent with the results by the Madey group which attributed these two states to the dissociated and first monolayer water adsorption, respectively. A recent study by Lu et al.[71] demostrated that, in addition to the molecular and dissociative adsorption, water molecules can be reduced at the Ti^{3+} sites on the $TiO_2(110)$ surface to produce hydrogen gas. The oxygen atom in the water molecule is preferentially extracted by the substrate to fill the surface oxygen vacancies. This selective reduction process (as well as others) can be used to infer the relative coverage of oxygen vacancy defect sites.[71]

The interaction of water with other single-crystal TiO_2 surfaces as well as powdered TiO_2 has also been investigated. Bustillo et al.[72] and Lo et al.[73] studied the thermal desorption of water from the $TiO_2(100)$ surface and reported dissociative adsorption of water. On powdered TiO_2, three TPD peaks can be observed. A poorly resolved doublet at ~211 K was attributed to multilayer and monolayer adsorption. A 311 K desorption peak was assigned to a different form of molecularly adsorbed H_2O, and a 568 K desorption was thought to arise from dissociatively adsorbed H_2O. The production of hydrogen gas was also detected for H_2O adsorption on reduced TiO_2 powder,[74] indicating that the reduction property is characteristic of the Ti^{3+} defect sites.

3.2.2. H_2 Adsorption

Göpel et al.[75] studied the adsorption of hydrogen on the $TiO_2(110)$ surface using temperature programmed desorption (TPD), electron paramagnetic resonance (ESR), and measurements of surface conductivity $(\Delta\sigma)$ and work function $(\Delta\varphi)$. The surface defect sites (oxygen vacancies) were found to act as electron donors and are the specific sites for H_2 adsorption. Chemisorption of hydrogen at 300 K forms ionic titanium hydride bonds $Ti^{4+}-H^-$ after H_2 dissociative adsorption at the defect sites. This process involves the transfer of two electrons which before adsorption were attributed to one oxygen vacancy site (with two Ti^{3+} present). These two hydrogen atoms can easily recombine during subsequent thermal desorption measurements, exhibiting first-order desorption kinetics. The adsorbed hydrogen atoms also diffuse into the bulk at 300 K, causing a nearly linear increase in conductivity $(\Delta\sigma)$ when the $TiO_2(110)$ crystal is exposed to a continuous flow of molecular hydrogen. An initial sticking coefficient of 1×10^{-6} was reported for H_2 adsorption on TiO_2-(110) at 300 K. In the absence of surface defects, the

activation energy to dissociate the H_2 molecule is too high, and no adsorption was observed.

A recent study by Pan et al.[69] also reported a very low sticking probability for H_2 adsorption on TiO_2-(110). Low-energy H_2^+ ion bombardment was employed to enhance the hydrogen adsorption. Surface hydroxyl groups were generated upon hydrogen ion exposures. In addition, the surface Ti^{3+} coverage was found to increase with increasing hydrogen exposures.

On powdered TiO_2 surfaces, Beck et al.[76] reported TPD spectra typical of weakly adsorbed molecular hydrogen. Iwaki[77] observed different adsorption behavior for hydrogen on anatase and on rutile TiO_2. On both types of TiO_2 powders, chemisorption of hydrogen took place only when hydrogen was introduced above 623 K.

3.2.3. Oxygen Adsorption

Partial charge transfer from the surface adsorption site to the oxygen molecule was found to play an important role for oxygen adsorption on $TiO_2(110)$. On the basis of conductivity $(\Delta\sigma)$ and surface potential $(\Delta\varphi)$ measurements, Göpel et al.[75] proposed the formation of O_2^- upon chemisorption of oxygen. This step requires the presence of surface defect sites, and is the precursor for further dissociative reactions between the adsorbed O_2 and the surface or bulk oxygen vacancies. The initial sticking coefficient is $\sim 8 \times 10^{-5}$ at 300 K. The maximum desorption rate for oxygen thermal desorption occurs at $\sim$ 348 K.

Low-energy ion scattering study by Pan et al.[69] indicated that oxygen adsorption on $TiO_2(110)$ occurs at the surface oxygen vacancy sites. With the use of isotope $^{18}O_2$ adsorption, it was found that no oxygen adsorption would occur on a stoichiometric surface. Kurtz et al.[68] reported that oxygen was dissociated on the surface at 400 K and that the surface Ti^{3+} sites can be eliminated upon oxygen exposure. Lu et al.[78] found that oxygen molecularly adsorbs on $TiO_2(110)$ at 105 K, and all O_2 molecules are dissociated above 400 K.

Beck et al. studied the adsorption of oxygen on powdered rutile TiO_2 using thermal desorption measurements.[79] Three different desorption states at 164 K, 416 and $\sim$ 445 K were identified. Isotope labeling experiments showed no involvement of lattice oxygen in the 164 and 416 K desorption states, and only 7% lattice oxygen was detected in the high temperature peak. For oxygen adsorption on anatase TiO_2 powder, only the low temperature state was observed. A recent thermal desorption study by Yanagisawa et al.[80] reported a similar thermal desorption profile for O_2 on rutile TiO_2. Two desorption features at 180 and 470 K involved only the oxygen from gas adsorption while another desorption state at 520 K included oxygen from both the gas and the lattice.

3.2.4. CO and CO_2 Adsorption

Ab initio molecular orbital calculations by Kobayashi et al.[81] showed that CO weakly interacts with a defect-free $TiO_2(110)$ surface. The presence of oxygen vacancy defects strongly enhances such interactions due to electron back-donation from surface Ti^{3+} into the π^* orbitals of molecular CO. CO does

not adsorb onto the surface oxygen atoms. Carbonate ion type or colinear carbon dioxide precursor type surface complexes do not exist on the TiO$_2$ surface containing adsorbed CO. At 300 K, Göpel et al.[75] found that CO adsorbs only at the defect sites. A small amount of CO$_2$ can be formed due to the reaction of adsorbed CO with an adjacent bridging-oxygen atom, resulting in an additional oxygen vacancy. On a single-crystal TiO$_2$(110) surface, Lu et al.[78] reported a weakly bound CO state desorbing at $\sim$150 K. No thermal dissociation or oxidation was observed.

On a powdered rutile TiO$_2$ surface, Beck et al.[79] observed two CO desorption states at 175 and 437 K. These states were attributed to CO molecules interacting with the surface oxygen anions through the C-end of CO and CO molecules interacting with the surface defect sites through the O-end of CO, respectively. Infrared spectroscopic studies by Tanaka and White[82] observed two different molecularly adsorbed CO species with vibrational frequencies at 2185 and 2115 cm^{-1}. The lower frequency species was more strongly bound to the surface.

Göpel et al.[75] also reported that CO$_2$ weakly adsorbed on the TiO$_2$(110) surface and its adsorption was not influenced by the density of surface defect sites. In the presence of surface hydroxyl groups, Tanaka and White[82] found that CO$_2$ readily reacted to form bicarbonate species on a powdered anatase TiO$_2$ surface.

3.2.5. NO and SO$_2$ Adsorption

Lu et al.[71] studied the adsorption of NO on the TiO$_2$(110) surface and reported a weakly bound molecular adsorption state desorbing at 120 K. In addition, the reduction product, N$_2$O, was observed to desorb at 169 and 250 K. The 169 K desorption feature was observed only on defective surfaces and its intensity was proportional to the surface defect coverage. This low-temperature N$_2$O state was then associated with the NO reductive reaction at surface oxygen vacancy sites, e.g., NO$_{(a)}$ + vacancy $\rightarrow$ N$_{(a)}$ + O$_{lattice}$; N$_{(a)}$ + NO$_{(a)}$ $\rightarrow$ N$_2$O. These defect sites were completely removed upon oxidation by adsorbed NO (to produce N$_2$O).

Similar results were reported by Boccuzzi et al.[83] for NO adsorption on powdered TiO$_2$ using FT-IR measurements. NO weakly adsorbs on fully oxidized TiO$_2$ at 300 K. On the reduced sample, several molecular and dissociative adsorption states were identified. NO adsorption reoxidized the reduced sample. Thermal desorption measurements by Pande et al.[84] observed both NO and N$_2$O desorption from NO-exposed TiO$_2$ samples reduced at 523 K. Increasing the reduction temperature (and therefore the defect density) resulted in a higher yield of reduction products (N$_2$O and N$_2$). Only N$_2$O and N$_2$ were desorbed from an NO-exposed sample that was reduced at 1073 K.

Smith et al.[85] have shown that SO$_2$ also reacts with and oxidizes the oxygen vacancy sites (Ti^{3+}) on TiO$_2$(110) and Ti$_2$O$_3$(10$\bar{1}$2) surfaces. This reaction continued until all such defect sites were removed by SO$_2$ dissociation. Very weak interaction was observed for SO$_2$ on the nearly perfect TiO$_2$(110)

surface. Onishi et al.[86] investigated the adsorption of SO$_2$ on TiO$_2$(110) and (441) surfaces using X-ray and ultraviolet photoemission spectroscopies (XPS and UPS). On the (441) surface, SO$_2$ oxidized Ti^{3+} to Ti^{4+} accompanied with the formation of S^{2-} species. Only SO$_3{}^{2-}$ was detected upon SO$_2$ adsorption on the (110) surface at 300 K.

3.2.6. NH$_3$ and H$_2$S Adsorption

Diebold et al.[87] studied the NH$_3$ adsorption on TiO$_2$-(110) using XPS and low-energy ion scattering (LEIS). A saturation coverage of $\sim$ 0.16 ML [1 ML = 1 NH$_3$ per surface atom] was measured on the stoichiometric surface. A slightly higher coverage (0.19 ML) was observed on the highly defective surface. Ammonia adsorbs on TiO$_2$(110) in molecular form. Roman et al.[88] investigated the same adsorption system using synchrotron radiation UPS. It was found that ammonia weakly adsorbs at 300 K. The uptake was reported to be slightly higher on the perfect surface than on the defective surface. The surface species are predominately molecular ammonia. A small fraction possibly dissociates at the defect sites upon heating the surface to higher temperatures. The saturation coverage is $\sim$ 0.1 ML at 300 K.

Roman and de Segovia[89] also investigated the adsorption of ammonia on the TiO$_2$(001) surface using UPS and TPD. Similar to that found on the (110) surface, NH$_3$ molecularly adsorbed on TiO$_2$ (001) at 300 K. Molecular NH$_3$ desorbed at $\sim$338 K with first-order kinetics. Some ammonia was dissociated to produce NH$_2$ and OH species. Further decomposition of these products yields desorption of N$_2$ and H$_2$ at 343 and 364 K, respectively.

Smith et al.[90] studied the interaction of H$_2$S with a highly defective TiO$_2$(110) surface and identified two distinct adsorption states. At low coverages, H$_2$S dissociated to produce H and S atoms bound to surface Ti cation sites. The presence of the adsorbed sulfur atoms dramatically inhibited the oxidation of Ti^{3+} sites by oxygen adsorption. At high H$_2$S exposures, molecular adsorption was observed. This adsorption state can be thermally desorbed before 423 K. Beck et al.[79] studied the adsorption of H$_2$S on both anatase and rutile powders. Two molecularly adsorbed states (multilayer and monolayer) were observed in thermal desorption spectra on both anatase and rutile. A third irreversible adsorption state was observed only on rutile TiO$_2$ and was attributed to dissociative adsorption at bridge-bonding defect sites.

3.2.7. Deoxygenation Reactions of Organic Molecules on TiO$_2$

On TiO$_2$ surfaces, various coordinatively unsaturated Ti cations (Ti^{3+}, Ti^{2+}, and Ti^{1+}) can be generated by vacuum annealing, Ar$^+$ sputtering, or chemical reductions (using H$_2$ or CO).[68,69,75,91] It is the relative ease in producing such defect sites that makes the TiO$_2$ surface exhibit not only the acid–base properties of most metal oxides, but also oxidation–reduction reactivities. This is particularly true for the adsorption of oxygen-containing organic molecules which commonly undergo dehydration, dehydrogenation, deoxygenation, and self-disproportionation reactions.

E_{vac} 0

$-4.2V$ ---- H_2/H_2O

$1.23V$

O_2/H_2O

$3.2\,eV$
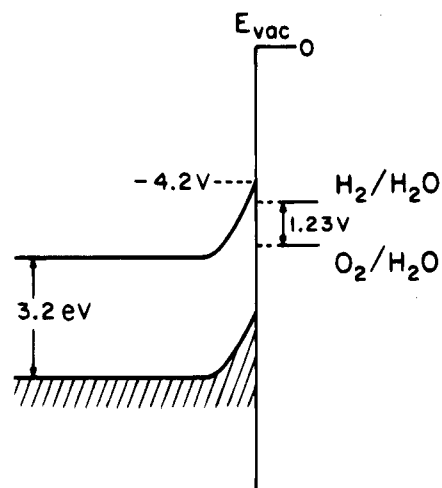
Figure 3.5. Potential energy diagram for the H_2/H_2O and O_2/H_2O redox couples relative to the band-edge positions for TiO_2.

The deoxygenation of alcohols,[92,93] carboxylic acids,[94] ketones,[95] and aldehydes[96] have been observed on reduced $TiO_2(100)$ and TiO_2 powder surfaces. Olefins (RCH=CHR) are produced by the reductive coupling of aldehyde (RCH=O) molecules at the oxygen vacancy defect sites. Ethylene formation was observed upon formaldehyde adsorption on a defective $TiO_2(110)$ surface.[71] The yield of ethylene production was directly correlated to the coverage of surface defect sites. On a reduced $TiO_2(100)$ surface, formaldehyde decomposes to adsorbed C, H, and O, which further react upon heating to higher temperatures to produce methoxide species, CO, and CO_2.[91] On the fully oxidized (100) surface, formaldehyde undergoes a Cannizzaro-type reaction to simultaneously produce adsorbed methoxide and formate species.[91] The yield of each product is strongly dependent on the preparation procedure of the surface. The formation of dioxymethylene ($-OCH_2O-$) has been observed during formaldehyde adsorption on TiO_2.[97,98] Among all the above-mentioned adsorption processes, the deposition or removal of surface oxygen atoms play an essential role.

3.3. Photochemistry of Small Inorganic Molecules on TiO_2

3.3.1. Photodecomposition of Water on TiO_2

Even though TiO_2 can be effectively photoexcited under band-gap irradiation, H_2O cannot be photodecomposed on clean TiO_2 surfaces. Figure 3.5 illustrates the band-edge positions of TiO_2 relative to the electrochemical potentials of the H_2/H_2O redox couple and the O_2/H_2O redox couple.[99] According to this electron energy diagram, water photolysis is energetically favorable. However, due to the presence of a large overpotential for the evolution of H_2 and O_2 on the TiO_2 surface, TiO_2 alone becomes inactive. Although earlier studies by Schrauzer et al.[100] reported the photosplitting of water using TiO_2, Sato and White[74] demonstrated that the hydrogen evolution from wet TiO_2 is not due to the photocatalytic splitting of water, but rather the photoassisted oxidation of the oxygen vacancy sites on reduced TiO_2. Sustained photodecomposition of water has

$H_2O \xrightarrow[Pt-TiO_2]{h\nu} H_2 + \frac{1}{2}O_2$
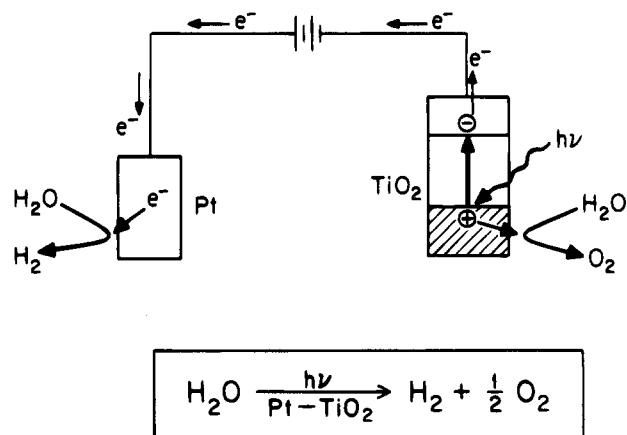
Figure 3.6. Photosplitting of water in a photoelectrochemical cell.

$H_2O \xrightarrow[RuO_2-TiO_2-Pt]{h\nu} H_2 + \frac{1}{2}O_2$
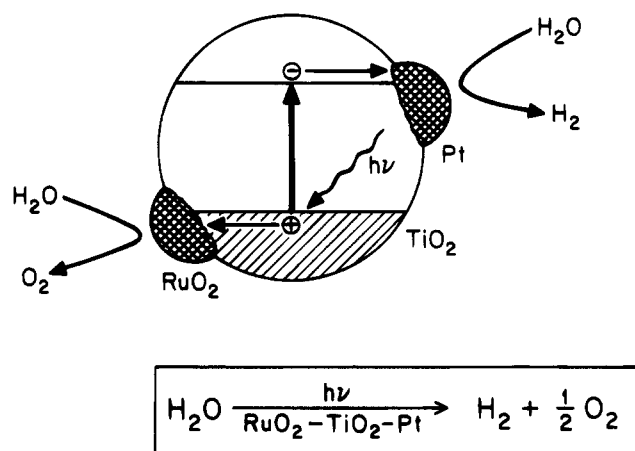
Figure 3.7. Photosplitting of water on composite catalyst.

been achieved under each of the following experimental conditions. Here, each experimental configuration is designed to effectively separate the photogenerated electrons and holes for maximum photoreaction yield.

(1) A closed circuit photoelectrochemical cell employing a TiO_2 anode and a metal (Pt in most cases) cathode, as shown in Figure 3.6. Here, hydrogen evolves from Pt and oxygen from TiO_2. A small externally applied electrical potential $(>0.25\ V)$[101] may be necessary but this is much smaller than that required in an electrochemical cell for H_2O electrolysis $(>1.23\ V)$. Such photoelectrochemical configurations were extensively studied in the 1970s and early 1980s.[2-6] The system was designed to resemble an electrochemical reaction and to effectively separate the photogenerated electrons and holes. The photoexcitation of TiO_2 injects electrons from its valence band into its conduction band. The electrons flow through the external circuit to the Pt cathode where water molecules are reduced to hydrogen gas and the holes remain in the TiO_2 anode where water molecules are oxidized to oxygen.

(2) TiO_2 powders with deposited metal particles (such as Pt) for H_2 evolution and metal oxide particles (such as RuO_2) for O_2 evolution,[102] as shown in Figure 3.7. Here, this system behaves as a short-circuited micro photoelectrochemical cell in which Pt is the cathode and RuO_2 is the anode. Band-gap excitation in the TiO_2 substrate injects negatively charged
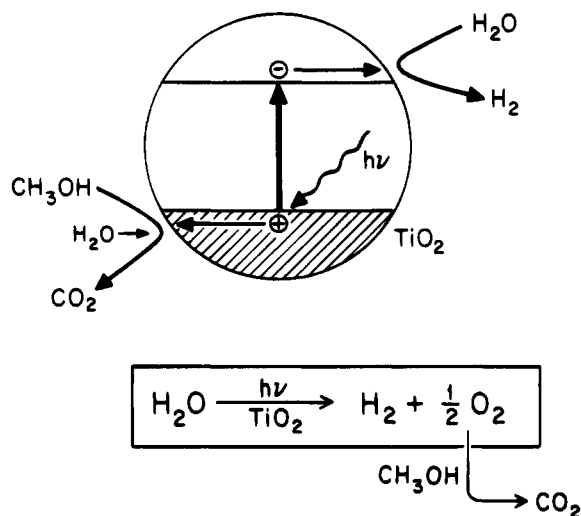
Figure 3.8. Photosplitting of water: sacrificial donor effect.

electrons into the Pt particles and positively charged holes into the RuO_2 particles. Trapped electrons in Pt reduce water to hydrogen and trapped holes in RuO_2 oxidize water to oxygen. The presence of Pt and RuO_2 significantly reduces the overpotential for H_2 and O_2 production, respectively.

(3) The use of sacrificial species to remove one of the photodecomposition products so that the reaction equilibrium is shifted toward further decomposition, as shown in Figure 3.8. Here, the sacrificial species may be oxidized by the hole-reaction product (presumably O_2) or reduced by the electron-reaction product (presumably H_2). For example, when alcohols such as CH_3OH are added to a TiO_2 aqueous suspension, sustained H_2 production is observed upon UV irradiation and the alcohol molecules are oxidized to CO_2.[103] Additional examples about the photooxidation and reduction processes in aqueous TiO_2 systems will be given later in this section.

The detailed mechanism for the photodecomposition of water on TiO_2 and the photooxidation or reduction reactions involving the water–TiO_2 system remains a controversial issue today. A number of researchers have reported the observation of several radical species using EPR measurements. Gonzalez-Elipe et al.[104] reported the formation of $HO_2\cdot$ and $\cdot O^-$ or $\cdot O_2^{3-}$ species generated by UV irradiation of hydrated anatase TiO_2 in oxygen. Anpo and coworkers[105] observed $\cdot OH$ radicals at 77 K on hydrated anatase under band-gap irradiation. Jaeger and Bard reported the formation of $HO_2\cdot$ and $\cdot OH$ radicals in aqueous suspensions of TiO_2.[99] Howe and Grätzel[31] observed that surface hydration of anatase has a significant influence on the reactivity of holes and electrons generated upon band-gap irradiation. Trapped electrons are readily scavenged by adsorbed oxygen. Trapped holes are much less reactive, and they react with surface hydroxyl groups above 77 K to produce $\cdot O_2^-$. Hydroxyl radicals are not the primary products and their existence is transient.

3.3.2. Photoadsorption and Photodesorption of Oxygen on TiO₂

The photoadsorption and photodesorption of O_2 on TiO_2 have been investigated in an effort to under-

stand the electron charge transfer from the substrate to oxygen during adsorption and to understand the electron scavenging process by oxygen during photooxidation of organics. Early investigations of photoadsorption were in fact dealing with the photooxidation of organic contaminants on the TiO_2 surface by the photoactivated oxygen.[106] Carbon dioxide was formed in most of these adsorption studies. It was believed that the photooxidation occurs through the formation of O_2^- radical ions. Courbon et al.[107] suggested the formation of O^- and O_3^- ($O_2 + O^-$) as the intermediates for photooxidation and photoisotope exchange reactions. Bickley et al.[108] and Munuera et al.[104,109] studied the photoadsorption of oxygen on rutile TiO_2 surfaces and found that the presence of adsorbed water enhances the photoadsorption of oxygen by trapping the photogenerated holes at OH^- sites. The formation of surface HO_2^- by electron trapping ($H^+ + O_2 + 2e^- \rightarrow HO_2^-$) and O_3^- by hole trapping reactions ($O^{2-}_{(lattice)} + O_2 + h^+ \rightarrow O_3^-$) is the primary route for O_2 photoadsorption.

Oxygen adsorption is an important step for the photocatalytic oxidation of organics on TiO_2. Anpo et al.[110] showed that O_3^- was formed by the reaction of O^- (hole trap, $O^{2-}_{(lattice)} + h^+ \rightarrow O^-$) with adsorbed oxygen molecules, as discussed above. These authors also demonstrated the exclusive incorporation of gas phase oxygen into the CO_2 product upon CO photooxidation on TiO_2, that is, $^{18}O_2 + C^{16}O \rightarrow 2C^{16}O^{18}O$. No lattice oxygen was involved. Their calculations implied that the photoactivation of oxygen occurred by the formation of a O_3^- ($^{18}O-^{18}O-^{16}O^-$) species in which the $O-O$ bond in the original O_2 molecule is significantly weakened.

Oxygen photodesorption from powdered TiO_2 was recently studied by Yanagisawa and Ota.[80] It was found that the photodesorption occurs only when photon energy above the TiO_2 band gap was delivered. Oxygen desorbed molecularly, and no isotopic exchange with the lattice was observed. The photodesorption signal followed $t^{-1/2}$ decay kinetics, similar to that observed for CO_2 photodesorption from ZnO.[111] These rate kinetics were attributed to the recombination of adsorbed O_2^- (or CO_2^- on ZnO) with the photogenerated holes.

Lu et al.[78] studied the adsorption of oxygen on a $TiO_2(110)$ surface and similar desorption behavior was observed. No isotopic mixing was detected during the photodesorption experiments even when a mixture of $^{18}O_2$ and $^{16}O_2$ was adsorbed on the surface.

3.3.3. Photooxidation and Photoreduction of Molecular Nitrogen

The photocatalytic activity of TiO_2 for N_2 oxidation and reduction have been observed by several researchers. Schrauzer et al.[100] first reported the photoreduction of N_2 by an iron-doped TiO_2 catalyst. Adsorbed water was photodecomposed to yield oxygen, and at the same time nitrogen was reduced to produce NH_3 and N_2H_4. The hydrogenation of unsaturated hydrocarbons was also achieved photocatalytically in the same study.

Bickley and co-workers[112] studied the photooxidation of N_2 on TiO_2 at the gas–solid interface. Ther-
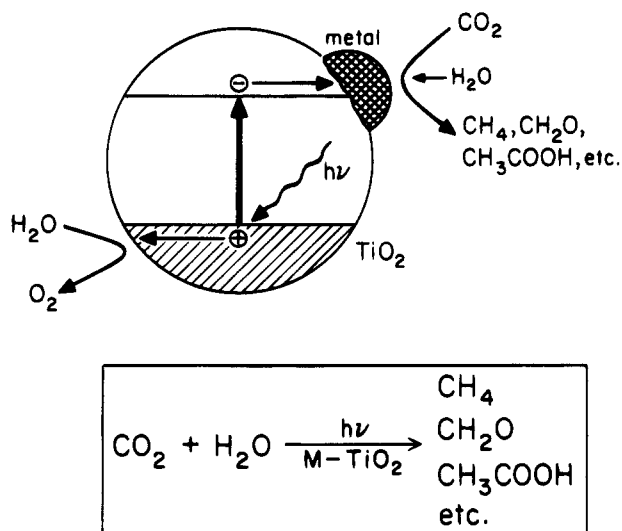
Figure 3.9. Photosplitting of water: sacrificial acceptor effect.

mal desorption of NO was detected at ~640 K after irradiating a mixture of N_2 and O_2 in the presence of hydroxylated TiO_2 at 300 K. A $N_2O_2^{2-}$ species was suggested as the photooxidation product on the surface based on comparative thermal desorption and X-ray photoemission studies. Further oxidation of this species to nitrite and nitrate ions is possible.

3.3.4. Photoreduction of CO2

The photoreduction of CO_2 is an important process since it is a naturally occurring photobiological process and can be achieved electrochemically. Inoue et al.[113] first reported that a suspension of TiO_2 photocatalyzes the reduction of CO_2 with water to produce formic acid, formaldehyde, methanol, and a trace amount of methane. Studies by Hirano et al.[114] observed methanol as the main photoreduction product from CO_2 when a Cu-containing TiO_2 suspension was irradiated. Several researchers have designed experiments to enhance the efficiency and selectivity for CO_2 photoreduction. The presence of Hg or Pt seemed to accelerate the formation of formaldehyde or carbon.[115] Ishitani and co-workers systematically investigated the effect of different metals on the photoreduction selectivity, and reported that methane and acetic acid are the major products when Pd, Rh, Pt, Au, Cu, or Ru were deposited onto TiO_2 catalysts.[116] The Pd–TiO_2 system exhibited very high selectivity for the production of methane from CO_2 photoreduction. The process can be schematically illustrated in Figure 3.9.

3.3.5. Photooxidation of Halides on TiO2

Flash photolytic oxidation of halides on TiO_2 were first conducted on colloidal TiO_2 particles. In the time-resolved study by Draper and Fox,[117] iodide oxidation was monitored on TiO_2 powders and a direct hole-adsorbate electron transfer process was suggested. The one-electron oxidation intermediate I_2^- (or Br_2^-, Cl_2^-) was detected by several research groups. The formation of I_2^- was studied by Fitzmaurice et al.[118] by photoirradiation of aqueous I^- solution on TiO_2 colloidal particles. It was found that the photogenerated electrons and holes each get

trapped at surface or subsurface sites. A trapped hole reacts with an adsorbed I^- ion to form an I atom which further reacts with I^- to produce I_2^-:

$$I^- + h^+ \rightarrow I \qquad I + I^- \rightarrow I_2^- \qquad 2I_2^- \rightarrow I_3^- + I^- \tag{9}$$
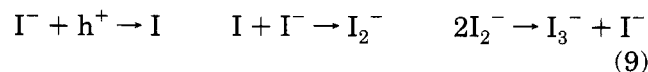
In the presence of oxygen, electrons are effectively removed by transfering to adsorbed oxygen. The I_2^- will then disproportionate to form I_3^- and I^-. When there is no oxygen or other efficient electron scavenger present, trapped electrons will eventually recombine with the holes trapped in I_2^- to give back I^- ions:

$$I_2^- + e^- \rightarrow 2I^- \tag{10}$$

The photoinduced oxidation of halide on TiO_2 electrodes was also reported.[119]

### 3.3.6. Photoinduced Surface Corrosion

Photogenerated electrons and holes diffuse to the surface region and are trapped at surface or subsurface sites where interfacial electron transfer takes place to induce oxidation and reduction reactions. However, if these trapped charge carriers are not quickly removed through such reactions, irreversible chemical changes will occur to the semiconductor surface layer itself. Studies have shown that both surface and bulk defects in TiO_2 and ZnO can be produced upon photoirradiation.[111] Changes in color or electrical conductivity are generally good parameters for evaluating the extent of photocorrosion. For example, TiO_2 electrodes in contact with solution became dark after repeated exposure to UV irradiation.[120] TiO_2 dissolution occurred under these conditions. However, no such change was observed in the absence of irradiation. Metal sulfides are especially easy to corrode upon prolonged photoexposure.[121,122]

3.4 Photooxidation on TiO2 Single Crystals

The photochemical reaction on a TiO_2 catalyst is generally believed to involve radical species. The extensive research on photodecomposition of water and photooxidation of organics has provided some evidence for such intermediates. However, some important issues regarding the reactive sites, the roles of each individual reactant species, and the detailed mechanisms remain unsettled. Single-crystal surfaces provide the opportunity to study a well-ordered structure with known surface area and controlled surface coverages of the reactant molecules and the surface reactive sites.

3.4.1. Photoelectrochemistry on Single-Crystal Electrodes

Photoelectrochemistry using TiO_2 electrodes was one of the most active area of research in the 1970s and early 1980s.[2,3] Most of the research interests emphasized the photoelectrolysis of water to produce hydrogen and oxygen. The close connection between electrochemistry and photocatalysis lies in the fact that both processes involve interfacial electron transfer (driven by electrical potentials or by photons, respectively). Most of the fundamental concepts in photoinduced heterogeneous electron transfer were either derived from some existing principles of elec-
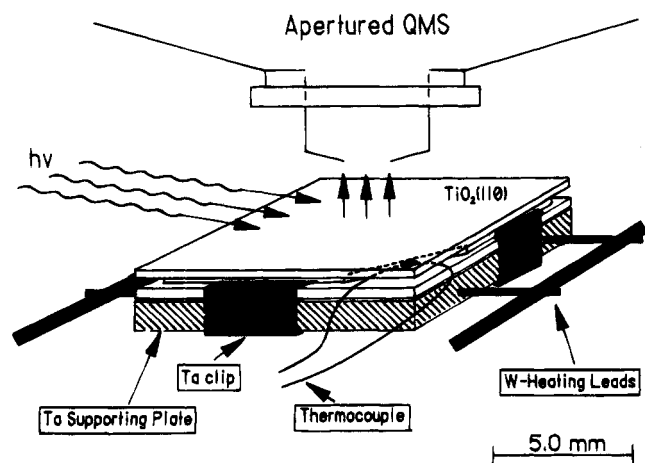
Figure 3.10. Design of crystal holder for photochemistry on TiO$_2$(110) single crystal.

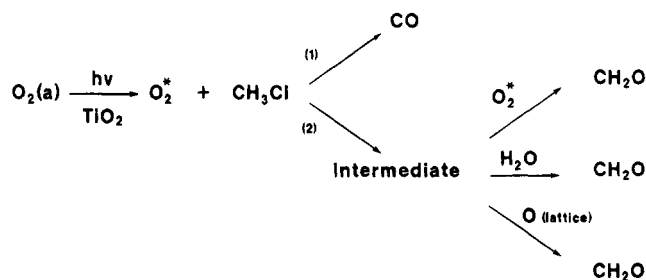**Figure 3.11.** Summary of CH$_3$Cl photooxidation on TiO$_2$-(110).

trochemistry or based on photoelectrochemical measurements. Single-crystal semiconductor electrode materials are most likely to represent the ideal situation of interfacial electron transfer processes.

Studies in this field have been presented in several excellent reviews and textbooks,[2-6] and shall not be repeated here. However, we do wish to point out some recent photoelectrochemical studies on the electron transfer process directly related to the photooxidation of toxic waste on TiO$_2$. Using a single-crystal TiO$_2$(001) electrode for photoelectrochemical measurements, Kesselman et al.[123] were able to independently evaluate the interfacial charge transfer reactions for the electrons and for the holes. The electron transfer rate constant (10^{-7} cm/s) obtained in this study suggested that, when the photooxidation of CHCl$_3$ by oxygen is conducted in aqueous solution using 30 nm TiO$_2$ particles (typical size for catalyst particles used in real applications), the interfacial charge transfer (and not the electron–hole generation) is the rate-limiting step for the overall photodegradation process.

3.4.2. Photochemical Studies on Single-Crystal TiO₂

The only UHV surface science study for the photodegradation of organic pollutants concerns the photooxidation of CH$_3$Cl on the rutile TiO$_2$(110) surface.[66] The method for mounting the TiO$_2$ single crystal, reproducibly heating it, and studying photodesorption and photooxidation processes using a line-of-sight mass spectrometer is indicated by Figure 3.10. Here an oriented and polished single crystal of TiO$_2$ is mechanically clipped to a Ta supporting plate. The plate may be heated by ohmic heating of the W-heating leads which are mounted inside the plate. Feedback control from the thermocouple, embedded in a corner slot, permits linear temperature programming of the crystal. The apertured mass spectrometer (QMS) may be used to monitor photodesorption directly or to monitor the adsorbed photoproducts liberated during temperature programmed desorption. The aperture selectively collects desorbing species from the center of the crystal.

The roles of surface defect sites produced in a controlled and reproducible manner by carefully timed annealing cycles, adsorbed oxygen, and ad-

sorbed water were characterized using surface science techniques. It was found that surface Ti^{3+} sites (oxygen vacancies) are the active sites for the photocatalytic oxidation of methyl chloride. Molecular oxygen adsorbed at such sites was activated by charge transfer of electrons that were produced due to band-gap excitation of TiO$_2$. The activated oxygen species were the primary oxidizing agents and react with methyl chloride to produce CO, HCl, formaldehyde, and water. Adsorbed water and hydroxyl groups participated in the reaction only after the photooxidation was initiated by the activated oxygen. Isotopic labeling of molecular oxygen indicated that adsorbed oxygen was exclusively incorporated into CO (100%) and extensively into formaldehyde (70%). The oxygen in the water or the TiO$_2$ lattice was only partially incorporated into formaldehyde (30%). The photooxidation reaction exhibited a threshold energy of $\sim$3.1 eV, the band gap of rutile TiO$_2$. This study clearly demostrated that under UHV conditions substrate-mediated photoactivation of adsorbed oxygen is the key step in the photocatalytic oxidation of methyl chloride on TiO$_2$(110). Figure 3.11 schematically shows the mechanism proposed for this oxidation process, where O$_2$* is a generalized symbol for an activated species whose identity is currently unknown.

In comparison to the study of photooxidation on single crystal TiO$_2$(110), Wong et al.[124] conducted a parallel FT-IR study of methyl chloride photooxidation on powdered TiO$_2$. Consistent results were obtained which support the conclusions made in the single-crystal study. Gas phase oxygen must be present for the reaction to occur, and it was this oxygen that was incorporated into the oxidation products. However, the final product from powdered TiO$_2$ catalysts was CO$_2$, not CH$_2$O. Carbon monoxide, which contained exclusively the oxygen from the gas phase oxygen, was also detected as a reaction intermediate and was further oxidized into CO$_2$. The difference in the photooxidation products on powdered TiO$_2$ compared to TiO$_2$(110) was attributed to the presence of more or different reactive sites on the powdered TiO$_2$ which contains both anatase and rutile (as compared to the single-crystal rutile surface), which allow the oxidation to occur to a larger extent. It is also possible that the powdered TiO$_2$ studies involved a greater surface concentration of O$_2$(a) due to the higher pressure used compared to the TiO$_2$(110) studies in UHV.
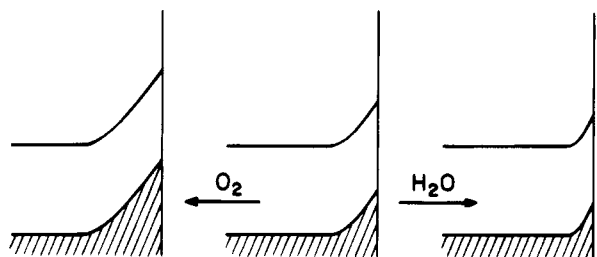
Figure 3.12. Schematic description of the surface band-bending changes: effects of H_2O and O_2 adsorption.

3.5. Photooxidation at the Gas–Solid Interface on TiO₂ Catalysts

3.5.1 Introduction

In recent years, one of the most active areas of research in photocatalysis concerns environmental decontamination, namely the photomineralization of organic pollutants.[125] TiO_2 is used in such studies as the photocatalyst for both gas phase and aqueous suspension systems. The research efforts have aimed at two major photooxidation issues: (1) the identification of reaction intermediates, detailed reaction mechanisms, and reaction kinetics; and (2) the optimization of reaction conditions to enhance the photoreaction rate and yield. The photooxidation in aqueous suspensions will be summarized in section 3.6. Here, a few representative reactions will be discussed for gas phase photooxidation on TiO_2 catalysts. Among all the gas–solid photooxidation reactions, trichloroethylene (TCE) and chlorophenols (CP) have been most extensively investigated.[8] The oxidation intermediates and the influence of water and oxygen on the overall reaction kinetics have been determined.

3.5.2. The Photoactivity of TiO₂: Effects of Adsorbed H₂O and O₂

Anpo et al.[126] recently studied the influence of water and oxygen on the photocatalytic activity of TiO_2. It was found that the adsorption of water on the TiO_2 surface caused a decrease in the upward band bending (as shown in Figure 3.12), and therefore an increase in the efficiency for the recombination of photogenerated electrons and holes. This is because in this case the barrier height and width is smaller for the return of a surface trapped electron into the bulk conduction band region. On the other hand, addition of O_2 led to an increase in the upward band bending, and therefore suppressed the electron–hole recombination processes leading to more efficient photoactivity. The above conclusions were based on the observed photoluminescense enhancement by H_2O adsorption and photoluminescence quenching by O_2 adsorption. From a chemical point of view, the adsorbed water then can be regarded as an effective electron–hole recombination center while the adsorbed oxygen can be considered as an effective electron trap to prevent such a recombination process. These results have important implications for gas phase photooxidation processes on TiO_2. Some of the observed kinetics can be explained using these concepts.

3.5.3. Trichloroethylene (TCE)

TCE is a common pollutant in air and water due to its wide use as a solvent in industry. The final
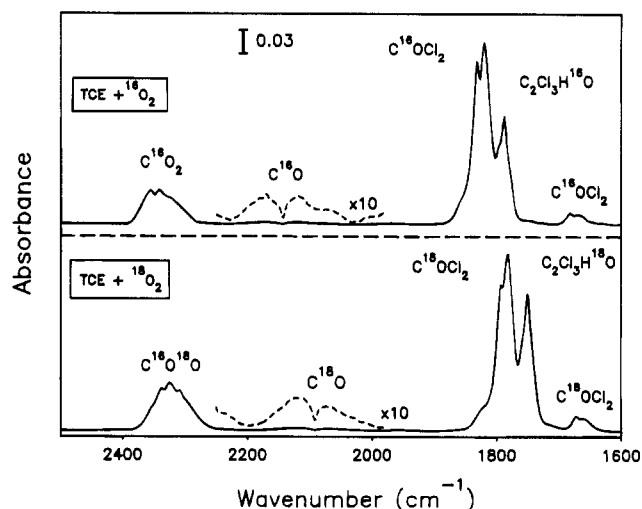
Figure 3.13. Isotopic shifts in the infrared spectra of TCE photooxidation gas products on TiO_2 at 300 K.

photooxidation products for TCE on TiO_2 are CO_2, CO, HCl, and Cl_2. For gas phase photooxidation, phosgene ($COCl_2$), dichloroacetyl chloride (DCAC, $CHCl_2COCl$), and sometimes dichloroacetyl acid ($CHCl_2COOH$) in the presence of excess water, have been identified as the oxidation intermediates by several independent research groups.

Phillips and Raupp[127] studied the reaction kinetics and found that in the absence of water vapor, the TiO_2 catalyst exhibited a high initial photoactivity which then declined rapidly with time. At low water vapor pressure, the photooxidation rate is independent of the water partial pressure, whereas at higher partial pressure the reaction rate is strongly inhibited by the water vapor. Oxygen showed second-order kinetics which shifted to zeroth order with increasing oxygen pressure. On the basis of the kinetics data, the authors suggested that the photoproduction of hydroxyl radical ($\cdot OH$) and hydroperoxide radicals ($HO_2\cdot$, $\cdot O_2^-$) was the rate-determining step. However, it was not determined which radical species attacked the TCE molecule and induced the photooxidation.

Fan et al.[128] studied this reaction using isotopically labeled oxygen and water. Similar reaction intermediates and products were identified (that is, DCAC, phosgene, CO, CO_2 and surface carboxylate groups). Figure 3.13 shows the isotope induced vibrational frequency shifts in these compounds in the gas phase when TCE is oxidized by oxygen ($^{18}O_2$ or $^{16}O_2$) on hydroxylated TiO_2. It is quite obvious that only oxygen atoms from the gas phase oxygen are incorporated into the intermediates (DCAC, phosgene, CO), while isotope mixing occurs in CO_2. This is probably due to the formation of carboxylates on the surface (which involve lattice ^{16}O as an intermediate for the release of final product, CO_2). Therefore, the initial oxidation of TCE involved exclusively the gas phase O_2-derived active radical species ($HO_2\cdot$, $\cdot O_2^-$, etc.) and not the hydroxyl radicals from direct hole trapping by surface hydroxyl groups.

Larson and Falconer[129] analyzed the surface composition of the TiO_2 catalysts during and after TCE photooxidation reactions. Their results implied that the accumulation of Cl ions and other reaction intermediates may poison the TiO_2 catalyst for

further TCE photooxidation; the presence of water (either vapor or liquid) helped to remove these surface species.

3.5.4. 4-Chlorophenol (4-CP)

Photodegradation of 4-chlorophenol has been investigated in gas phase,[130] in aqueous suspension,[131-133] and on electrodes.[134] The molecule is of interest due to its benzene ring structure which allows the capture of radical intermediates (such as •OH) or the direct interaction with an electron. A recent FT-IR study of the gas phase reaction by Stafford et al.[130] found that in the absence of water vapor, 4-CP was photooxidized possibly by reacting with the photogenerated $\cdot O_2^-$ radical species. Addition of water vapor to the system dramatically enhanced the rate and extent of photooxidation. However, the exact cause for this change was not determined. Direct reaction of 4-CP with photogenerated electrons was also observed. 4-CP accepts one electron and releases one Cl^- ion, resulting in hydroquinone formation. Futher photooxidation required the presence of oxygen. From these results, the authors pointed out that hydroxyl radicals (•OH) may not be exclusively responsible for the photooxidation of 4-CP and the role of oxygen is more than that of merely an electron scavenger.

3.6. Photooxidation at the Liquid–Solid Interface on TiO₂ Catalysts

3.6.1. Introduction

By using TiO₂ as a catalyst, the photooxidation of organics may be used for decontamination treatment in polluted waters. Such applications have inspired a vast amount of research. The solid photocatalysts studied include colloidal particles, high surface area powders, and single-crystal surfaces. The complexity of the liquid–solid interface presents many more variables (in comparison to the gas–solid system) to be dealt with in kinetics studies. Such parameters include the surface composition, surface area, preparation procedures, and concentration of the photocatalyst; the pH of the solution and its effect on the surface structure; the concentration of the reactants; the solvent environment; the partial presure of oxygen; the diffusion rate in solution and near the surface, etc. Care must be taken with the controllable parameters, or discrepencies will occur in the experimental results. For instance, chlorobenzene was first reported not to undergo complete mineralization over TiO₂.[135] However, experiments with a differently prepared TiO₂ catalyst and with a higher oxygen pressure demonstrated that total photooxidation of chlorobenzene may be achieved.[136] The various kinetic parameters in the liquid–solid photooxidation systems have been discussed in several recent reviews.[14-19]

3.6.2. The Primary Events of Photooxidation at the Liquid–Solid Interface

Continuous band-gap irradiation of an aqueous semiconductor dispersion excites an electron from the valence band to the conduction band, creating an electron–hole pair. The electrons possess the reduc-

ing power of the conduction band energy and the holes have the oxidizing power of the valence band energy. From the band-edge positions of the valence band and conduction band, as discussed in section 2.2.2, the redox capability of a photoexcited semiconductor particle in the aqueous solution can be estimated. The bulk photoelectrons and photoholes can recombine to produce thermal energy, or rapidly migrate to the surface and react with adsorbed species at the surface. In a steady state photocatalytic reaction, the rate of oxidation by the holes has to be balanced by the rate of reduction by the electrons. Either of these reactions can be rate determining.

Although the above physical events are generally accepted as the initial step for the photooxidation process, the subsequent chemical events at the liquid–solid interface remain an ambiguous and controversial issue. The trapped holes have been proposed to directly oxidize adsorbate molecules,[117] or to react with surface hydroxyl groups to produce hydroxyl radicals which are strong oxidizing agents.[137] The chemical identification of hydroxylated oxidation intermediates and the ESR detection of hydroxyl radicals appear to support the hydroxyl radical mechanism. However, these data do not permit the unambiguous delineation of the •OH-driven mechanism versus the direct hole oxidation mechanism since similar reaction intermediates are expected from these two schemes in an aqueous system. A recent diffuse reflectance flash photolysis experiment in nonaqueous solution presented evidence in favor of the direct hole oxidation route.[117] The trapped electrons are believed to react with preadsorbed molecular oxygen to produce O_2^- and O_2^{2-} anions. However, the ultimate fate of these activated oxygen species was not determined. They may directly oxidize organic species, protonate to generate hydroperoxide radicals and hydroxyl radicals, or further react with more trapped electrons to eventually form water. Recent studies of 4-chlorophenol (4-CP) degradation in a TiO₂ slurry suggested that oxygen plays a specific role during photooxidation in addition to scavenging the trapped electrons.[130,138,139] It was found that 4-CP degradation only occurs to a small extent (20%) in the presence of an alternative electron acceptor capable of sweeping up trapped electrons as readily as oxygen, while complete photomineralization is achieved in a similar time frame when oxygen is present.

3.6.3. The Dynamics of Charge Carrier Trapping, Recombination, and Interfacial Electron Transfer

In an aqueous solution, picosecond and nanosecond laser photolysis was employed to investigate the dynamics of charge carrier trapping and recombination in ~ 60 Å colloidal particles of TiO₂.[30] The trapping of the conduction band electrons is a very rapid process and occurs within 30 ps. By contrast, the trapping of the valence band holes is a much slower process requiring an average time of 250 ns. The recombination of trapped electrons with free or trapped holes takes place in the 10^{-11} to 10^{-6} s time domain. At low charge carrier concentration, the mean lifetime of a single electron–hole pair is ~30

ns in a semiconductor particle, and the hole trapping can compete with the recombination process. In the trapped state, holes are relatively unreactive toward electrons.[30] At a high concentration of electron—hole pairs, the charge carriers recombine within a fraction of one nanosecond. Therefore, the interfacial carrier trapping must be very rapid in order to achieve effective photochemical conversion. This requires the electron or hole trapping species to be preadsorbed on the catalyst surface.

Gerischer and co-workers[140] recently analyzed the photooxidation kinetics of organic molecules on TiO_2 particles in aqueous environment. It was found that the rate of photooxidation is equal to and limited by the reduction rate of dissolved oxygen (O_2) in the solution. It was theoretically predicted[140] and experimentally confirmed[141] that when O_2 is not reduced at a sufficiently high rate, electrons accumulate on the photocatalyst particles, and the rate of radiationless recombination is enhanced until the sum of the electron—hole recombination and the electron transfer to O_2 is equal to the rate of the hole photogeneration. The deposition of Pd metal particles on TiO_2 enhances the electron transfer to O_2 and eliminates the electron accumulation on the TiO_2 particles.

3.6.4. Overview of Photomineralization Reactions in Aqueous Semiconductor Dispersions

In an aqueous TiO_2 suspension, the holes in the TiO_2 valence band have enough oxidizing power to convert any organic species to CO_2, water, and mineral acids (such as HCl). The photogenerated holes in the semiconductor particles, the hole-trapping radical species, and the activated oxygen species (by electron trapping) are all strong oxidation agents for organic compounds. The nonselective and total photooxidation property of the system has been applied for water purification by the photomineralization of organic pollutants. Almost every major class of organic contaminant has been examined for possible degradation using this technique. Detailed mechanistic analysis of these reactions have appeared in several recent reviews[8,13-19] and shall not be repeated here.

4. Surface Modifications

4.1. Introduction

As was stated earlier in this review, one of the most active fields of research in heterogeneous photocatalysis using semiconductor particles is the development of a system capable of using natural sunlight to degrade a large number of organic and inorganic contaminants in wastewater.[8,142-144] The overall photocatalytic activity of a particular semiconductor system for the stated purpose is measured by several factors including the stability of the semiconductor under illumination, the efficiency of the photocatalytic process, the selectivity of the products, and the wavelength range response. For example, small band-gap semiconductors such as CdS are capable of receiving excitation in the visible region of the solar spectrum, but are usually unstable and photodegrade
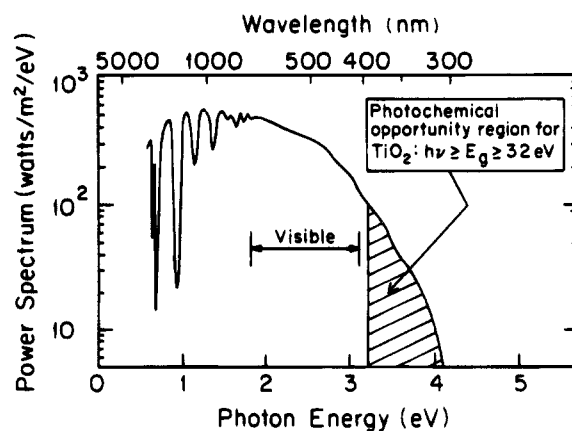
Figure 4.1. Solar spectrum at sea level with the sun at zenith.

with time.[121] On the other hand, TiO_2 is a quite stable photocatalyst, but since the band gap is large ($E_g = 3.2$ eV) it is only active in the ultraviolet region which is <10% of the overall solar intensity as shown in Figure 4.1.[145]

The limitations of a particular semiconductor as a photocatalyst for a particular use can be surmounted by modifying the surface of the semiconductor. To date, three benefits of modifications to photocatalytic semiconductor systems have been studied: (1) inhibiting recombination by increasing the charge separation and therefore the efficiency of the photocatalytic process; (2) increasing the wavelength response range (i.e. excitation of wide band gap semiconductors by visible light); and (3) changing the selectivity or yield of a particular product. A few examples will be given in the following sections illustrating the large body of work conducted in the area of photocatalyst surface modification.

4.2. Metal Semiconductor Modification

In photocatalysis the addition of noble metals to a semiconductor can change the photocatalytic process by changing the semiconductor surface properties. The metal can enhance the yield of a particular product or the rate of the photocatalytic reaction. The enhancement in reactivity was first observed for the photoconversion of H_2O to H_2 and O_2 using the Pt/TiO_2 system.[146] The addition of a metal to a semiconductor surface can also change the reaction products.

Figure 4.2 is an illustration of the electron capture properties at the Schottky barrier of the metal in contact with a semiconductor surface. The picture schematically illustrates the small area of the semiconductor surface that the metal actually covers. Transmission electron microscopy measurements have found that when the added metal is Pt, the Pt particles form clusters on the surface.[147] With a Pt dose of 10 wt %, only 6% of the semiconductor surface area is covered. Therefore a large surface area of the semiconductor is still exposed.

After excitation the electron migrates to the metal where it becomes trapped and electron—hole recombination is suppressed. The migration of electrons to the metal particles was confirmed by studies showing the reduction in the photoconductance of the
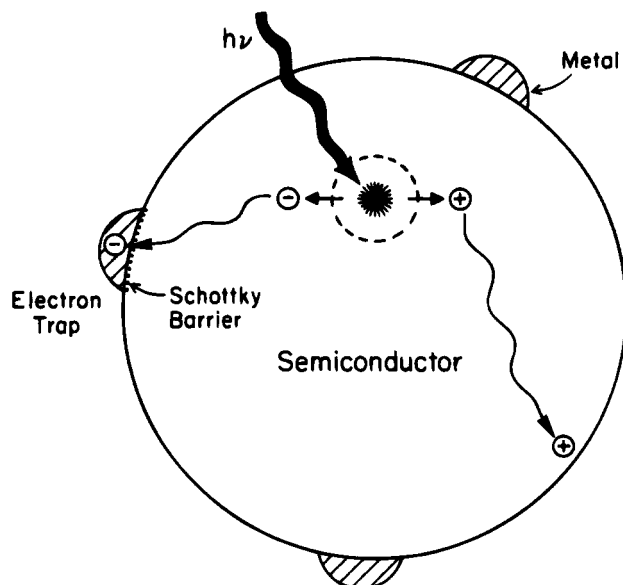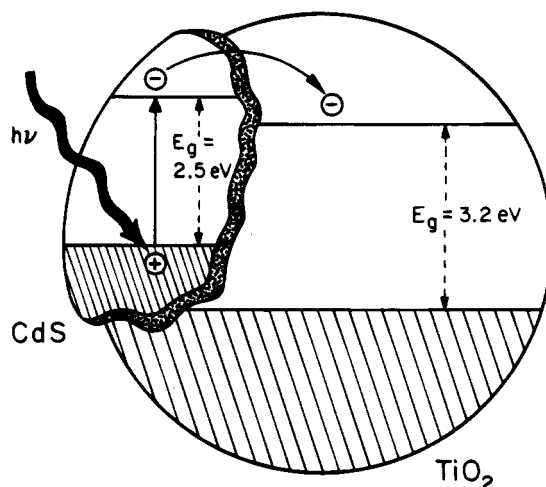
Figure 4.2. Metal-modified semiconductor photocatalyst particle.

Figure 4.3. Photoexcitation in composite semiconductor–semiconductor photocatalyst.

semiconductor for the Pt deposited TiO_2 compared to TiO_2 alone.[148a] The hole is then free to diffuse to the semiconductor surface where oxidation of organic species can occur.

The Pt/TiO_2 system is the metal–semiconductor system most commonly studied. As was previously stated, the photostability of TiO_2 and the capability of band-gap excitation in the solar region make it the semiconductor of choice. The addition of Pt to the TiO_2 surface is beneficial for photocatalytic reactions evolving gas, especially hydrogen. The metal is important also because of its own catalytic activity. The metal actually modifies the photocatalytic properties of the semiconductor by changing the distribution of electrons. The effect of added metal to the semiconductor's electronic properties was explained in section 2.2.5. When the two species come in contact the Fermi levels of the metal and semiconductor align causing electrons to flow to the metal from the semiconductor. The decrease in electron density within the semiconductor leads to an increase in the hydroxyl group acidity.[148b] This in turn affects the photocatalytic process on the semiconductor surface.

The electronic modification of the semiconductor surface via metal deposition can also be observed with other noble metals. The addition of silver to the TiO_2 surface does increase the production of H_2 from alcohol. The increase in H_2 production is attributed to the trapping of electrons at the metal sites. The increase in H_2 production for the Ag/TiO_2 photocatalyst is not as great as the increase in H_2 production for Pt/TiO_2.[149]

TEM has determined that the size of Pt particles remained the same over the 0.5–10% Pt range of content on the TiO_2 surface. The Pt particles have a mean diameter of 2 nm.[147] There is an optimum loading of Pt (1.0 wt %) to achieve a maximum photocatalytic rate of hydrogen production from alcohols. This shows that the morphology or geometrical factor does not affect the photocatalytic properties of the mixed system but an optimum Pt

content affects the distribution of electrons in the system. Above the optimum metal content the efficiency of the photocatalytic process actually decreases. Care must be taken when studies are conducted on a metal-modified semiconductor to work with the quantity of metal which gives the optimum photocatalytic efficiency.

4.3. Composite Semiconductors

Coupled semiconductor photocatalysts provide an interesting way to increase the efficiency of a photocatalytic process by increasing the charge separation, and extending the energy range of photoexcitation for the system. Figure 4.3 illustrates geometrically and energetically the photoexcitation process for the composite (coupled) semiconductor–semiconductor photocatalyst $CdS–TiO_2$. Transmission electron micrographs of the coupled semiconductors shows the direct geometrical interaction of multiple CdS particles with the TiO_2 particle surface.[149] The relative positions of the conduction and valence band energy levels for the two semiconductors are referenced to the vacuum level (see Figure 2.4). The energy of the excitation light is too small to directly excite the TiO_2 portion of the photocatalyst, but it is large enough to excite an electron from the valence band across the band gap of CdS ($E_g = 2.5eV$) to the conduction band. According to this energetic model in Figure 4.3, the hole produced in the CdS valence band from the excitation process remains in the CdS particle while the electron transfers to the conduction band of the TiO_2 particle. The electron transfer from CdS to TiO_2 increases the charge separation and efficiency of the photocatalytic process. The separated electron and hole are then free to undergo electron transfer with adsorbates on the surface. The quantum yield for the reduction of methylviologen drastically increased and approached an optimum value of 1 when the concentration of TiO_2 was increased in a $CdS–TiO_2$ system.[150]

Transient absorption spectra of the composite $CdS–TiO_2$ photocatalyst indicate trapping of the electron at Ti^{4+} sites on the TiO_2 surface. The $CdS–TiO_2$ system exhibits a broad absorption band in the 550–750 nm region after receiving a 355 nm (3.5 eV)
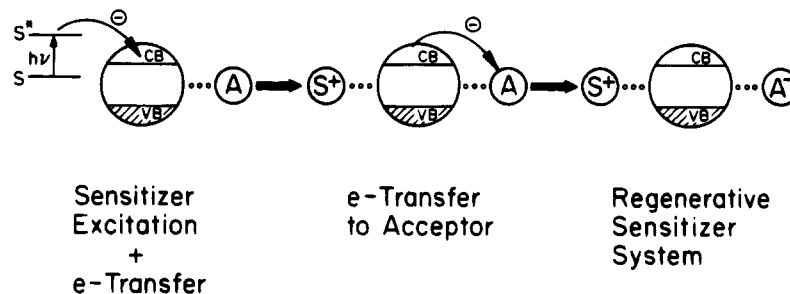
Figure 4.4. Excitation steps using dye molecule sensitizer.

picosecond laser pulse. This band is characteristic of chemical changes associated with the trapping of electrons on the TiO_2 surface. The lack of absorption activity in the 550–750 nm region was tested by using the same laser pulse with the TiO_2 particles alone. Only the CdS portion of the composite photocatalyst exhibited an absorption band in the visible region. The transient absorption spectrum showed no absorption on clean TiO_2. The experimental results show that the coupling of semiconductors with the appropriate energy levels can produce a more efficient photocatalyst via better charge separation.

4.4. Surface Sensitization

Surface sensitization of a wide band-gap semiconductor photocatalyst (TiO_2) via chemisorbed or physisorbed dyes can increase the efficiency of the excitation process. The photosensitization process can also expand the wavelength range of excitation for the photocatalyst through excitation of the sensitizer followed by charge transfer to the semiconductor.[151] Some common dyes which are used as sensitizers include erythrosin B,[152] thionine,[153] and analogs of $Ru(bpy)_3^{2+}$.[154,155]

Figure 4.4 illustrates the excitation and charge injection steps involved for the regenerative dye sensitizer surface process. Excitation of an electron in the dye molecule occurs to either the singlet or triplet excited state of the molecule (see Figure 2.2). If the oxidative energy level of the excited state of the dye molecule with respect to the conduction band energy level of the semiconductor is favorable (i.e. more negative), then the dye molecule can transfer the electron to the conduction band of the semiconductor. The surface acts as a quencher accepting an electron from the excited dye molecule. The electron in turn can be transferred to reduce an organic acceptor molecule adsorbed on the surface. A study has been conducted which demonstrates the reduction of N,N,N',N'-tetraethyloxonine by a sensitized TiO_2 system. The sensitizer was anthracene-9-carboxylic acid which extended the response of TiO_2 into the visible region, $\lambda = 450$ nm.[156] In this system a redox couple was employed to regenerate the dye sensitizer. Without the presence of a redox couple, the dye sensitizer semiconductor system can also be used in oxidative degradation of the dye sensitizer molecule itself after charge transfer. This is important due to the large quantity of dye substances in wastewater from the textile industries.

4.5. Transition Metal Doping

The influence of dissolved transition metal impurity ions on the photocatalytic properties of TiO_2 has

become another interesting area of semiconductor modification. The benefit of transition metal doping species is the improved trapping of electrons to inhibit electron–hole recombination during illumination. With Fe^{3+} doping of TiO_2, an increase in Ti^{3+} intensity was observed by ESR upon photoirradiation due to trapped electrons.[157] Only certain transition metals such as Fe^{3+} [158] and Cu^{2+} [158,159] actually inhibit electron–hole recombination. The concentration of the beneficial transition metal dopants is very small and large concentrations are detrimental. Other transition metal dopants such as Cr^{3+} [160] create sites which increase electron–hole recombination. It is believed that these transition metals create acceptor and donor centers where direct recombination occurs. Compared to the other areas of surface modification, the amount of work conducted on the photoreaction of different organic species with transition metal doped TiO_2 systems is very small.

5. Summary

In a heterogeneous photocatalysis system, the efficiency for chemical transformation depends on the photoactivity of the adsorbate molecules and the catalyst substrates. In the case of an inert oxide substrate, electron transfer or energy transfer events occur between the adsorbate molecules. The catalyst only provides an ordered environment for a more efficient molecular interaction and does not participate in the photoexcitation or chemical reaction process. The chemical reactions induced by photon absorption and the subsequent relaxation is determined by the nature of the adsorbate molecular structure.

In the case of a reactive semiconductor substrate, the catalyst can either provide energy levels to mediate electron transfer between adsorbate molecules (by temporarily accommodating an electron) or behave as both an electron donor (the photogenerated electron in the conduction band) and an electron acceptor (the photogenerated hole in the valence band). Here, the band structure of the substrate plays a significant role. A change in the surface and bulk electronic structure can dramatically alter the chemical events following photoexcitation of the adsorbate molecules or the catalyst substrate.

Applications of heterogeneous photocatalysis to environmental cleanup involve the use of photocatalysts for the non-selective total oxidation of organic pollutants. TiO_2 is photoactive in the UV region (<400 nm) and is currently considered the most promising catalyst for air and water photocatalytic

decontamination. Water and oxygen molecules are considered necessary for the photooxidation process, however, very different kinetics effects by these two surface species have been reported by different authors and for different compounds. For gas—solid systems, it has been shown that molecular oxygen is necessary for the photooxidation to occur while water is necessary to remove from the catalyst surface some of the reaction intermediates or products, the accumulation of which may poison the catalyst. For aqueous TiO_2 suspension systems, it is believed that the ·OH radicals from hole-trapping by surface hydroxyl groups are the primary oxidizing agents and oxygen is a scavenger for photogenerated electrons. However, for aqueous TiO_2 suspensions, there is currently no isotope labeling experiment to definitively show which species (H_2O or O_2) is more extensively incorporated into the photooxidation intermediates or products. Further studies are necessary to elucidate the mechanistic details of the photocatalytic process in the aqueous suspension system.

Electronic modification of the catalyst by deposition of metal particles, sensitizer molecules, or other semiconductor particles has a strong effect on the photoactivity of the system. The wavelength tuning of photoresponse, the efficiency of electron—hole separation, and the dynamics of interfacial electron transfer can be dramatically influenced. The application of these fundamental principles for designing photochemical transformation methods is a rich area for both basic scientific research and technological development.

6. Acknowledgments

7. References

(1) Fujishima, A.; Honda, K. *Nature* **1972**, *37*, 238.
(2) Bard, A. J. *J. Phys. Chem.* **1982**, *86*, 172; *J. Photochem.* **1979**, *10*, 59; *Science* **1980**, *207*, 139.
(3) Grätzel, M., Ed. *Energy Resources Through Photochemistry and Catalysis*; Academic Press: New York, 1983.
(4) Kalyanasundaram, K.; Grätzel, M.; Pelizzetti, E. *Coord. Chem. Rev.* **1986**, *69*, 57.
(5) Parmon, V. N.; Zamareav, K. I. In *Photocatalysis - Fundamentals and Applications*; Serpone, N., Pelizzetti, E., Eds.; Wiley Interscience: New York, 1989; p 565.
(6) Pelizzetti, E., Schiavello, M., Eds. *Photochemical Conversion and Storage of Solar Energy*; Kluwer Academic Publishers: Dordrecht, 1991.
(7) Schiavello, M., Ed. *Photocatalysis and Environment*; Kluwer Academic Publishers: Dordrecht, 1988.
(8) Ollis, D. F., Al-Ekabi, H., Eds. *Photocatalytic Purification and Treatment of Water and Air*; Elsevier: Amsterdam, 1993.
(9) Mauzerall, D.; Ballard, S. G. *Annu. Rev. Phys. Chem.* **1982**, *33*, 377.
(10) Forster, T. *Faraday Discuss. Chem. Soc.* **1959**, *27*, 7.
(11) Okabe, H. *Photochemistry of Small Molecules*; Wiley-Interscience: New York, 1978.
(12) Gilbert, A.; Baggott, J. *Essentials of Molecular Photochemistry*; CRC Press: Boca Raton, 1991.
(13) Fox, M. A., Chanon, M., Eds. *Photoinduced Electron Transfer, Part A: Conceptual Basis*; Elsevier: Amsterdam, 1988.
(14) Serpone, N., Pelizzetti, E., Eds. *Photocatalysis - Fundamentals and Applications*; Wiley-Interscience: New York, 1989.
(15) Grätzel, M. *Heterogeneous Photochemical Electron Transfer*; CRC Press: Boca Raton, 1989.
(16) Julliard, M.; Chanon, M. *Chem. Rev.* **1983**, *83*, 425.
(17) Kavarnos, G. J.; Turro, N. J. *Chem. Rev.* **1986**, *86*, 401.
(18) Fox, M. A.; Dulay, M. T. *Chem. Rev.* **1993**, *93*, 341.
(19) Kamat, P. V. *Chem. Rev.* **1993**, *93*, 267.
(20) Struve, W. S. *Fundamentals of Molecular Spectroscopy*; Wiley: New York, 1989.
(21) Atkins, P. W. *Molecular Quantum Mechanics*, 2nd ed.; Oxford University Press: Oxford, 1983.
(22) Cotton, F. A. *Chemical Applications of Group Theory*, 2nd ed.; Wiley: Chichester, 1971.
(23) Douglas, B. E.; Hollingsworth, C. A. *Symmetry in Bonding and Spectra: An Introduction*; Academic Press: San Diego, 1985.
(24) (a) Skoog, D. A. *Principles of Instrumental Analysis*; Saunders College Pub.: New York, 1971, p 228. (b) Peters, K. *Annu. Rev. Phys. Chem.* **1987**, *38*, 253.
(25) Kasha, M. *Discuss. Faraday Soc.* **1950**, *9*, 14.
(26) Nosaka, Y.; Fox, M. A. *J. Phys. Chem.* **1988**, *92*, 1893.
(27) Matthews, R. W. *J. Catal.* **1988**, *113*, 549.
(28) Gerischer, H. In *Photocatalytic Treatment of Water and Air*: Ollis, D. F., Al-Ekabi, H., Eds., Elsevier: Amsterdam, 1993.
(29) Spanhel, L.; Haase, M.; Weller, H.; Henglein, A. *J. Am. Chem. Soc.* **1987**, *109*, 5649.
(30) Rothenberger, G.; Moser, J.; Grätzel, M.; Serpone, N.; Sharma, D. K. *J. Am. Chem. Soc.* **1985**, *107*, 8054.
(31) Howe, R. F.; Grätzel, M. *J. Phys. Chem.* **1987**, *91*, 3906.
(32) Henglein, A. *Chem. Rev.* **1989**, *89*, 1861.
(33) Henglein, A. *Top. Curr. Chem.* **1988**, *143*, 113.
(34) Kubo, R.; Kawabata, A.; Kobayashi, S. *Annu. Rev. Mater. Sci.* **1984**, *14*, 49.
(35) Wang, Y. In *Photochemical Conversion and Storage of Solar Energy*; Pelizzetti, E., Schiavello, M., Eds., Kluwar Acad. Pub.: Dordrecht, 1991; p 295.
(36) Nozik, A. In *Photocatalytic Purification and Treatment of Water and Air*; Ollis, D. F., Al-Ekabi, H., Eds.; Elsevier Science Pub.: New York, 1993; p 39.
(37) Wang, Y.; Herron, N.; Mahler, W.; Suna, A. *J. Opt. Soc. Am. B* **1989**, *6*, 808.
(38) Steigerwald, M. L.; Brus, L. E. *Annu. Rev. Mater. Sci.* **1989**, *19*, 471.
(39) Brus, L. E. *J. Chem. Phys.* **1983**, *79*, 5566.
(40) Brus, L. E. *J. Chem. Phys.* **1984**, *80*, 4403.
(41) Koch, U.; Foitik, A.; Weller, H.; Henglein, A. *Chem. Phys. Lett.* **1985**, *122*, 507.
(42) Wang, Y.; Suna, A.; Mahler, W.; Kasawski, R. *J. Chem. Phys.* **1987**, *87*, 7315.
(43) Foitik, A.; Weller, H.; Koch, U.; Henglein, A. *Ber. Bunsen-Ges. Phys. Chem.* **1984**, *88*, 969.
(44) Weller, H.; Schmidt, H. M.; Koch, U.; Foitik, A.; Baral, S.; Henglein, A.; Kunath, W.; Weiss, K.; Diekmann, E. *Chem. Phys. Lett.* **1986**, *124*, 557.
(45) Schmidt, J. M.; Weller, H. *Chem. Phys. Lett.* **1986**, *129*, 615.
(46) Kayanuma, Y. *Phys. Rev. B* **1988**, *38*, 9797.
(47) Rhoderick, E. H.; Williams, R. H. *Metal-Semiconductor Contacts*, 2nd ed.; Oxford University Press: New York, 1988; p 11.
(48) Ramamurthy, V. *Photochemistry in Organized and Constrained Media*; VCH: New York, 1991.
(49) Gust, D.; Moore, T. A. *Science* **1989**, *244*, 35.
(50) Zhou, X.-L.; Zhu, X.-Y.; White, J. M. *Surf. Sci. Rep.* **1991**, *13*, 73.
(51) Rosenwaks, Y.; Thacker, B. R.; Nozik, A. J.; Ellingson, R. J.; Burr, K. C.; Tang, C. L. *J. Phys. Chem.* **1994**, *98*, 2739.
(52) Ford, W. E.; Rodgers, A. J. *J. Phys. Chem.* **1994**, *98*, 3822.
(53) Zhang, J. Z.; O'Neil, R. H.; Roberti, T. W. *J. Phys. Chem.* **1994**, *98*, 3859.
(54) Bedja, I.; Hotchandani, S.; Kamat, P. V. *J. Phys. Chem.* **1994**, *98*, 4133.
(55) Kamat, P. V.; Dimitrijevic, N. M.; Fessenden, R. W. *J. Phys. Chem.* **1988**, *92*, 2324.
(56) Rossetti, R.; Beck, S. M.; Brus, L. E. *J. Am. Chem. Soc.* **1984**, *106*, 980. Rossetti, R.; Brus, L. E. *J. Phys. Chem.* **1986**, *90*, 558.
(57) Lewis, N. S. *Annu. Rev. Phys. Chem.* **1991**, *42*, 543.
(58) Augustynski, J. *Electrochim. Acta* **1993**, *38*, 43.
(59) Burdett, J. K. *Inorg. Chem.* **1985**, *24*, 2244.
(60) Burdett, J. K.; Hughbands, T.; Gordon, J. M.; Richardson, J. W., Jr.; Smith, J. V. *J. Am. Chem. Soc.* **1987**, *109*, 3639.
(61) Fahmi, A.; Minot; C.; Silvi, B.; Causa, M. *Phys. Rev. B* **1993**, *47*, 11717.
(62) (a) Zschack. In *The Structure of Surfaces III*; Tong, S. Y., Van Hove, M. A., Takayanagi, K., Xie, X. D., Eds.; Springer Series In Surface Science, Vol. 24; Springer-Verlag Berlin: Heidelberg, 1991; p 646 and references therein. (b) Murray, P. W.; Leibsle, F. M.; Fisher, H. J.; Flipse, C. F. J.; Muryn, C. A.; Thornton, G. *Phys. Rev. B* **1992**, *46*, 12877. (c) Carroll, D. L.; Liang, Y.; Bonnell, D. A. *J. Vac. Sci. Technol. A* **1994**, *12* (4), 2298. (d) Poirier, G. E.; Hance, B. K.; White, J. M. *J. Phys. Chem.* **1993**, *97*, 5965; *J. Vac. Sci. Technol. B* **1992**, *10*, 6; *J. Phys. Chem.* **1993**, *97*, 6500.
(63) Henrich, V. E.; Kurtz, R. L. *Phys. Rev. B* **1981**, *23*, 6280. Henrich, V. E. *Rep. Prog. Phys.* **1985**, *48*, 1481.
(64) See, A. K.; Bartynski, R. A. *J. Vac. Sci. Technol. A* **1992**, *10*, 2591.
(65) Sanjines, R.; Tang, H.; Berger, H.; Gozzo, F.; Margaritondo, G.; Levy, F. *J. Appl. Phys.* **1994**, *75*, 2945.
(66) Lu, G.; Linsebigler, A.; Yates, J. T., Jr. *J. Phys. Chem.*, in press.

(67) Henrich, V. E.; Dresselhaus, G.; Zeiger, H. J. *Solid State Commun.* **1977**, *24*, 623.

(68) Kurtz, R. L.; Stockbauer, R.; Madey, T. E.; Roman, E.; de Segovia, J. L. *Surf. Sci.* **1989**, *218*, 178.

(69) Pan, J. M.; Maschhoff, B. L.; Diebold, U.; Madey, T. E. *J. Vac. Sci. Technol. A* **1992**, *10*, 2470.

(70) Hugenschmidt, M. B.; Gamble, L.; Campbell, C. T. *Surf. Sci.* **1994**, *302*, 329.

(71) Lu, G.; Linsebigler, A.; Yates, J. T., Jr. *J. Phys. Chem.* **1994**, *98*, 11733.

(72) Bustillo, F. J.; Roman, E.; de Segovia, J. L. *Vacuum* **1989**, *39*, 659; **1990**, *41*, 19.

(73) Lo, W. J.; Chung, Y. W.; Somorjai, G. A. *Surf. Sci.* **1978**, *71*, 199.

(74) Sato, S.; White, J. M. *J. Am. Chem. Soc.* **1980**, *102*, 7206; *J. Phys. Chem.* **1981**, *85*, 592.

(75) Göpel, W.; Rocker, G.; Feierabend, R. *Phys. Rev. B* **1983**, *28*, 3427.

(76) Beck, D. D.; White, J. M. *J. Phys. Chem.* **1984**, *88*, 174.

(77) Iwaki, T. *J. Chem. Soc., Faraday Trans. 1* **1983**, *79*, 137.

(78) Lu, G.; Linsebigler, A.; Yates, J. T., Jr. *J. Chem. Phys.* **1995**, *102*, 3005.

(79) Beck, D. D.; White, J. M.; Ratcliffe, C. T. *J. Phys. Chem.* **1986**, *90*, 3132.

(80) Yanagisawa, Y.; Ota, Y. *Surf. Sci. Lett.* **1991**, *254*, L433.

(81) Kobayashi, H.; Yamaguchi, M. *Surf. Sci.* **1989**, *214*, 466.

(82) Tanaka, K.; White, J. M. *J. Phys. Chem.* **1982**, *86*, 4708.

(83) Boccuzzi, F.; Guglielminotti, E.; Spoto, G. *Surf. Sci.* **1991**, *251/252*, 1069.

(84) Pande, N. K.; Bell, A. T. *J. Catal.* **1986**, *97*, 137.

(85) Smith, K. E.; Henrich, V. E. *Phys. Rev. B* **1985**, *32*, 5384. Smith, K. E.; Mackay, J. L.; Henrich, V. E. *Phys. Rev. B* **1987**, *35*, 5822.

(86) Onishi, H.; Aruga, T.; Egawa, C.; Iwasawa, Y. *Surf. Sci.* **1988**, *193*, 33.

(87) Diebold, U.; Madey, T. E. *J. Vac. Sci. Technol. A* **1992**, *10*, 2327.

(88) Roman, E. L.; de Segovia, J. L.; Kurtz, R. L.; Stockbauer, R.; Madey, T. E. *Surf. Sci.* **1992**, *273*, 40.

(89) Roman, E.; de Segovia, J. L. *Surf. Sci.* **1991**, *251/252*, 742.

(90) Smith, K. E.; Henrich, V. E. *Surf. Sci.* **1989**, *217*, 445.

(91) Idriss, H.; Kim, K. S.; Barteau, M. A. *Surf. Sci.* **1992**, *262*, 113.

(92) Kim, K. S.; Barteau, M. A.; Farneth, W. E. *Langmuir* **1988**, *4*, 533.

(93) Kim, K. S.; Barteau, M. A. *Surf. Sci.* **1989**, *233*, 13.

(94) Vohs, J. M.; Barteau, M. A. *Surf. Sci.* **1990**, *201*, 481.

(95) Kiennemann, A.; Idriss, H.; Kieffer, R.; Chaumette, P.; Durand, D. *Ind. Eng. Chem. Res.* **1991**, *30*, 1130.

(96) Idriss, H.; Pierce, K.; Barteau, M. A. *J. Am. Chem. Soc.* **1991**, *113*, 715. Idriss, H.; Kim, K. S.; Barteau, M. A. *J. Catal.* **1993**, *139*, 119.

(97) Lavalley, J.-C.; Lamotte, J.; Busca, G.; Lorenzeli, V. *J. Chem. Soc., Chem. Commun.* **1985**, 1006. Idriss, H.; Hindermann, J. P.; Kieffer, R.; Kiennemann, A.; Vallet, A.; Chauvin, C.; Lavalley, J. C.; Chaumette, P. *J. Mol. Catal.* **1987**, *42*, 205. Busca, G.; Lamotte, J.; Lavalley, J.-C.; Lorenzelli, V. *J. Am. Chem. Soc.* **1987**, *109*, 5197.

(98) Li, C.; Domen, K.; Maruya, K.-I.; Onishi, T. *J. Catal.* **1990**, *125*, 445.

(99) Jaeger, C. D.; Bard, A. J. *J. Phys. Chem.* **1979**, *83*, 3146.

(100) Schrauzer, G. N.; Guth, T. D. *J. Am. Chem. Soc.* **1977**, *99*, 7189.

(101) Wrighton, M. S.; Ginley, D. S.; Wolczanski, P. T.; Ellis, A. B.; Morse, D. L.; Linz, A. *Proc. Nat. Acad. Sci. U.S.A.* **1975**, 72 (4), 1518.

(102) Duonghong, D.; Borgarello, E.; Grätzel, M. *J. Am. Chem. Soc.* **1981**, *103*, 4685.

(103) Kawai, T.; Sakata, T. *J. Chem. Soc., Chem. Commun.* **1980**, 694.

(104) Gonzalez-Elipe, A.; Munuera, G.; Soria, J. *J. Chem. Soc., Faraday Trans. 1* **1979**, *75*, 749.

(105) Anpo, M.; Shima, T.; Kubokawa, Y. *Chem. Lett.* **1985**, 1799.

(106) Hieu, V. N.; Lichtman, D. *Surf. Sci.* **1981**, *103*, 535; *J. Catal.* **1982**, *73*, 329 and references therein.

(107) Courbon, H.; Formenti, M. Pichat, P. *J. Phys. Chem.* **1977**, *81*, 550.

(108) Bickley, R. I.; Stone, F. S. *J. Catal.* **1973**, *31*, 389. Bickley, R. I.; Munuera, G.; Stone, F. S. *J. Catal.* **1973**, *31*, 398.

(109) Munuera, G.; Rives-Arnau, V.; Saucedo, A. *J. Chem. Soc., Faraday Trans. 1* **1979**, *75*, 736.

(110) Anpo, M; Kubokawa, Y.; Fujii, T.; Suzuki, S. *J. Phys. Chem.* **1984**, *88*, 2572.

(111) Shapira, Y.; Cox. S. M.; Lichtman, D. *Surf. Sci.* **1976**, *54*, 43.

(112) Bickley, R. I.; Jayanty, R. K. M.; Navio, J. A.; Real, C.; Macias, M. *Surf. Sci.* **1991**, *251/252*, 1052 and references therein.

(113) Inoue, I.; Fujishima, A.; Konishi, S.; Honda, K. *Nature* **1979**, *277*, 637.

(114) Hirano, K.; Inoue, K.; Yatsu, T. *J. Photochem. Photobiol. A: Chem.* **1992**, *64*, 255.

(115) Tennakone, K. *Sol. Energy. Mater.* **1984**, *10*, 235. Rophael, W. M.; Malati, M. A. *J. Chem. Soc., Chem. Commun.* **1987**, 1418.

(116) Ishitani, O.; Inoue, C.; Suzuki, Y.; Ibusuki, T. *J. Photochem. Photobiol. A: Chem.* **1993**, *72*, 269.

(117) Draper, R. B.; Fox, M. A. *Langmuir* **1990**, *6*, 1396.

(118) Fitzmaurice, D. J.; Eschle, M.; Frei, H.; Moser, J. *J. Phys. Chem.* **1993**, *97*, 3806.

(119) O'Regan, B.; Grätzel, M. *Nature* **1991**, *353*, 737 and references therein.

(120) Kajeshwar, K.; Singh, P.; DuBow, J. *Electrochim. Acta* **1978**, *23*, 1117.

(121) Henglein, A. *J. Phys. Chem.* **1982**, *86*, 2291.

(122) Mills, G.; Zongguan, L.; Meisel, D. *J. Phys. Chem.* **1988**, *92*, 822.

(123) Kesselman, J. M.; Kumar, A.; Lewis, N. S. in *Photocatalytic Purification and Treatment of Water and Air*; Ollis, D. F., Al-Ekabi, H. Eds.; Elsevier: Amsterdam, 1993; p 19.

(124) Wong, J. C. S.; Linsebigler, A. L.; Lu, G.; Fan, J. F.; Yates, J. T., Jr. *J. Phys. Chem.* **1995**, *99*, 335.

(125) Blake, D. M. *Bibliography of Work on the Photocatalytic Removal of Hazardous Compounds from Water and Air*; U.S. Government Report, National Renewable Energy Laboratory, 1993.

(126) Anpo, M.; Chiba, K.; Tomonari, M.; Coluccia, S.; Che, M.; Fox, M. A. *Bull. Chem. Soc. Jpn.* **1991**, *64*, 543.

(127) Phillips, L. A.; Raupp, G. B. *J. Mol. Catal.* **1992**, 77, 297. Dibble, L. A.; Raupp, G. B. *Catal. Lett.* **1990**, *4*, 345; *Environ. Sci. Technol.* **1992**, *26*, 492.

(128) Fan, J. F.; Wong, J. C. S.; Yates, J. T., Jr. To be published.

(129) Larson, S. A.; Falconer, J. L. In *Photocatalytic Purification and Treatment of Water and Air*; Ollis, D. F., Al-Ekabi, H., Eds.; Elsevier: Amsterdam, 1993; p 473.

(130) Stafford, U.; Gray, K. A.; Kamat, P. V.; Varma, A. *Chem. Phys. Lett.* **1993**, *205*, 55. Gray, K. A.; Stafford, U.; Dieckmann, M. S.; Kamat, P. V. In *Photocatalytic Purification and Treatment of Water and Air*; Ollis, D. F., Al-Ekabi, H., Eds.; Elsevier: Amsterdam, 1993; p 455.

(131) Al-Ekabi, H.; Serpone, N. *J. Phys. Chem.* **1988**, *92*, 5726. Al-Ekabi, H.; Serpone, N.; Pelizzetti, E.; Minero, C.; Fox, M. A.; Draper, R. B. *Langmuir* **1989**, *5*, 250.

(132) Al-Sayyed, G.; D'Oliveira, J. C.; Pichat, P. *J. Photochem. Photobiol. A: Chem.* **1991**, *58*, 99.

(133) Cunnigham, J.; Sedlak, P. *J. Photochem. Photobiol. A: Chem.* **1994**, *77*, 255 and references therein.

(134) Vinodgopal, K.; Hotchandani, S.; Kamat, P. V. *J. Phys. Chem.* **1993**, *97*, 9040.

(135) Ollis, D. F.; Hsiao, C. Y.; Budiman, L.; Lee, C.-L. *J. Catal.* **1984**, *88*, 89.

(136) Matthews, R. W. *J. Catal.* **1986**, *97*, 565.

(137) Turchi, C. S.; Ollis, D. F. *J. Catal.* **1989**, *119*, 483; **1990**, *122*, 178.

(138) Matthews, R. W. *J. Catal.* **1988**, *111*, 264.

(139) Gerischer, H.; Heller, A. *J. Phys. Chem.* **1991**, *95*, 5261.

(140) Gerischer, H. *Electrochim. Acta* **1993**, 38, 3. Gerischer, H.; Heller, A. *J. Electrochem. Soc.* **1992**, *139*, 113.

(141) Wang, C. M.; Heller, A.; Gerischer, H. *J. Am. Chem. Soc.* **1992**, *114*, 5230.

(142) Ollis, D. F. *Environ. Sci. Technol.* **1985**, *19*, 480.

(143) Ollis, D. F.; Pelizzetti, E.; Serpone, N. *Environ. Sci. Technol.* **1991**, *25*, 1523.

(144) Matthews, R. W. *J. Phys. Chem.* **1987**, *91*, 3328.

(145) Jackson, J. D. *Classical Electrodynamics*; Wiley & Sons: New York, 1975; p 424.

(146) Sato, S.; White, J. M. *Chem. Phys. Lett.* **1980**, *72*, 83.

(147) Pichat, P.; Mozzanega, M.-N.; Disdier, J.; Herrmann, J.-M. *Nouv. J. Chim.* **1982**, *11*, 559.

(148) (a) Disdier, J.; Herrmann, J.-M.; Pichat, P. *J. Chem. Soc. Faraday Tran. 1* **1983**, *79*, 651. (b) Jaffrezic-Renault, N.; Pichat, P.; Foissy, A.; Mercier, R. *J. Phys. Chem.* **1986**, *90*, 2733.

(149) Sclafani, A.; Mozzanega, M.-N.; Pichat, P. *J. Photochem. Photobiol. A: Chem.* **1991**, *59*, 181.

(150) (a) Gopidas, K. R.; Bohorquez, M.; Kamat, P. V. *J. Phys. Chem.* **1990**, *94*, 6435. (b) Spanhel, L.; Weller, H.; Henglein, A. *J. Am. Chem. Soc.* **1987**, *109*, 6632.

(151) Gerischer, H.; Willig, F. *Top. Curr. Chem.* **1976**, *61*, 31.

(152) Kamat, P. V.; Fox, M. A. *Chem. Phys. Lett.* **1983**, *102*, 379.

(153) Patrick, B.; Kamat, P. V. *J. Phys. Chem.* **1992**, *96*, 1423.

(154) Vlachopoulos, N.; Liska, P. Augustynski, J.; Grätzel, M. *J. Am. Chem. Soc.* **1988**, *110*, 1216.

(155) Desilvestro, J.; Grätzel, M.; Kavan, L.; Moser, J.; Augustynski, J. *J. Am. Chem. Soc.* **1985**, *107*, 2988.

(156) Kamat, P. V. *J. Phys. Chem.* **1989**, *93*, 859.

(157) Grätzel, M.; Howe, R. F. *J. Phys. Chem.* **1990**, *94*, 2566.

(158) Butler, E. C.; Davis, A. P. *J. Photochem. Photobiol., A: Chem.* **1993**, *70*, 273.

(159) Fujihira, M.; Satoh, Y.; Osa, T. *Bull. Chem. Soc. Jpn.* **1982**, *55*, 666.

(160) Herrmann, J.-M.; Disdier, J.; Pichat, P. *Chem. Phys. Lett.* **1984**, *108*, 618.

CR940025E